



<i>Title:</i> NEON ATBD: NEON Imaging Spectrometer Level 1B Calibrated Radiance		<i>Date:</i> 03/25/2022
<i>NEON Doc. #:</i> NEON.DOC.001210	<i>Author:</i> W. Gallery	<i>Revision:</i> B

## NEON ALGORITHM THEORETICAL BASIS DOCUMENT: NEON IMAGING SPECTROMETER (NIS) LEVEL 1B CALIBRATED RADIANCE

PREPARED BY	ORGANIZATION	DATE
William Gallery	AOP	10/01/2013
Nathan Leisso	AOP	10/01/2013

APPROVALS	ORGANIZATION	APPROVAL DATE
Kate Thibault	SCI	03/25/2022

RELEASED BY	ORGANIZATION	RELEASE DATE
Tanisha Waters	CM	03/25/2022

See configuration management system for approval history.



<i>Title:</i> NEON ATBD: NEON Imaging Spectrometer Level 1B Calibrated Radiance		<i>Date:</i> 03/25/2022
<i>NEON Doc. #:</i> NEON.DOC.001210	<i>Author:</i> W. Gallery	<i>Revision:</i> B

## Change Record

REVISION	DATE	ECO #	DESCRIPTION OF CHANGE
A	06/16/2014	ECO-01260	Initial release
B	03/25/2022	ECO-06791	<ul style="list-style-type: none"><li>• Revised logo</li><li>• Minor formatting updates</li></ul>



Title: NEON ATBD: NEON Imaging Spectrometer Level 1B Calibrated Radiance		Date: 03/25/2022
NEON Doc. #: NEON.DOC.001210	Author: W. Gallery	Revision: B

**TABLE OF CONTENTS**

**1 DESCRIPTION.....1**

1.1 Purpose..... 1

1.2 Scope ..... 1

**2 RELATED DOCUMENTS AND ACRONYMS.....2**

2.1 Applicable Documents ..... 2

2.2 Reference Documents ..... 2

2.3 External References..... 2

2.4 Acronyms ..... 2

**3 DATA PRODUCT DESCRIPTION .....3**

3.1 Variables reported ..... 3

3.2 Input Dependencies ..... 3

3.3 Product Instances ..... 3

3.4 Temporal Resolution and Extent..... 3

3.5 Spatial Resolution and Extent..... 4

**4 SCIENTIFIC CONTEXT.....6**

4.1 Theory of Measurement/Observation..... 6

4.1.1 The NEON Imaging Spectrometer..... 6

4.1.2 Flight Operations..... 9

4.2 Theory of Algorithm .....12

4.2.1 Laboratory Calibration.....13

4.2.2 Science Data calibration .....16

**5 ALGORITHM IMPLEMENTATION.....29**

5.1 Processing Steps .....29

**6 UNCERTAINTY.....33**

6.1 Analysis of Uncertainty .....33

6.2 Reported Uncertainty.....38

**7 VALIDATION AND VERIFICATION.....40**

**8 SCIENTIFIC AND EDUCATIONAL APPLICATIONS .....41**

**9 FUTURE MODIFICATIONS AND PLANS .....42**

**10 BIBLIOGRAPHY.....43**



Title: NEON ATBD: NEON Imaging Spectrometer Level 1B Calibrated Radiance		Date: 03/25/2022
NEON Doc. #: NEON.DOC.001210	Author: W. Gallery	Revision: B

**11 APPENDIX A AOP ABBREVIATIONS AND GLOSSARY ..... 44**

**LIST OF TABLES AND FIGURES**

**Table 1.** Reported variables for data product NEON.*dom.site*.DP1.30005..... 3

**Table 2.** Input Dependencies ..... 3

**Table 3.** NIS operating sequence during a typical flight.....12

**Table 4.** Contents of row one of the frame data .....29

**Table 5.** Specifications of a row of frame data.....30

**Table 6.** Sources of uncertainty in the radiometric calibration .....34

**Table 7.** Sources of uncertainty in the spectral calibration of the imaging spectrometer.....37

**Table 8.** Abbreviations.....44

**Table 9.** Glossary .....46

**Figure 1.** Un-geolocated radiance displayed as an image. .... 4

**Figure 2.** Geolocated and regridded radiance displayed as an image..... 5

**Figure 3.** Optical ray trace through the NISDVU Spectrometer subsystem. .... 7

**Figure 4.** Annotated picture of the NIS focal plane (Ref. Hamlin et al. 2010)..... 8

**Figure 5.** Image of the NIS focal plane dark-offset. The dark-offset is the detector output with no illumination of the focal plane. .... 9

**Figure 6.** Flight path of the AOP flight over High Park, CO July 11, 2013. The color of the track indicates the altitude of the AOP above sea level.....10

**Figure 7.** Outlines of the AOP flight tracks for July11, 2013. The different colors outline the individual flight tracks.....11

**Figure 8.** Image plot of the flat field  $ff_{i,j}$  for NISDVU. ....14

**Figure 9.** Surface plot of the flat field  $ff_{i,j}$  for NISDVU extending the radiometric calibration coefficients to the entire Focal Plane Array (FPA). Spikes are indicative of poor or dead pixels. The extended sharp features at spectral pixels 273 and 399 result from order-sorting filters applied to the FPA.....15

**Figure 10.** Plot of the gain function  $G(s)$  for NISDVU.....15

**Figure 11.** Spectrometer data processing flowchart. ....17

**Figure 12.** The corrected response  $R_{i,j}$  to the OBC mid-level source: a. dark response, b. mid-level bright source, c. laboratory flat field, d. corrected response, e. spectral cross-section through d, f. spatial cross-section through d. ....19

**Figure 13.** Flow chart showing the calculation of the OBC bad pixel mask and flat field. ....20

**Figure 14.** The preliminary OBC flat field  $ff_1$  : a. preliminary flat field, b. spatial cross section through a, c. spectral cross-section through a.....21

**Figure 15.** The OBC bad pixel mask: a. OBC flat field, b. spatial cross-section through a., c. spectral cross-section through a.....22



Title: NEON ATBD: NEON Imaging Spectrometer Level 1B Calibrated Radiance		Date: 03/25/2022
NEON Doc. #: NEON.DOC.001210	Author: W. Gallery	Revision: B

**Figure 16.** OBC flat field with bad pixels removed: a. OBC flat field, b. spatial cross-section through a., c. spectral cross-section through a.....23

**Figure 17.** Dark pedestal shift: a. OBC dark calibration image, b. OBC mid-calibration image, c. the dark pedestal shift averaged over rows for the image in b.....24

**Figure 18.** Electric panel ghost: a. FPA frame showing expected illumination in area 1, b. horizontal cross section at the red line (line 300 of frame in a.) The red vertical lines in b delineate separate detector areas. A negative ghost is present in areas 2, 3, and 4 from the illumination in area 1. ....25

**Figure 19.** Spectral calibration of band centers: a. FPA frame with Hg area-lamp illuminating various spectral channels, b. Spectral trace along spatial column 300. ....26

**Figure 20.** Spectral pixel number vs wavelength. ....27

**Figure 21.** Normalized SRF for a single pixel compared to a modeled Gaussian SRF.....28

**Figure 22.** FWHM of SRF through the spectral channels of the FPA.....28

**Figure 23.** Sequence of the raw data for one flight line. ....30

**Figure 24.** Spectral uncertainty in the Spectralon reference panel BRF used in the radiometric calibration of the imaging spectrometer. ....34

**Figure 25.** Example of spectrally fitting Gaussians to Hg area-array lamp lines through spatial pixels (x-axis) covering the FOV. The y-axis is the spectral pixel number. ....35

**Figure 26.** Example of extending spectral calibration to remainder of FPA based on Hg area-array lamp results.....36

**Figure 27.** Normalized SRF for a single pixel compared to a modeled Gaussian SRF.....37

**Figure 28.** Radiometric calibration uncertainty based on the NIST traceable calibration protocol.....38

**Figure 29.** Spectral calibration uncertainties for pixel band-centers derived from spectrally calibrating the imaging spectrometer with Laser lines injected into an integrating sphere.....39

**Figure 30.** Orthorectification - each point (pixel) in the image is from a perpendicular (orthogonal) perspective. As you look down at each pixel it's as if you are looking straight down on that pixel. Left image is orthorectified; right is not.....47



<i>Title:</i> NEON ATBD: NEON Imaging Spectrometer Level 1B Calibrated Radiance		<i>Date:</i> 03/25/2022
<i>NEON Doc. #:</i> NEON.DOC.001210	<i>Author:</i> W. Gallery	<i>Revision:</i> B

## **1 DESCRIPTION**

### **1.1 Purpose**

This document details the algorithms used for creating the calibrated spectral radiance from the NEON Imaging Spectrometer (NIS) Level 0 data. It includes a detailed discussion of measurement theory and implementation, appropriate theoretical background, data product provenance, quality assurance and control methods used, approximations and/or assumptions made, and a detailed exposition of uncertainty resulting in a cumulative reported uncertainty for this product.

### **1.2 Scope**

This document describes the theoretical background and entire algorithmic process for creating the calibrated spectral radiance. It does not provide computational implementation details, except for cases where these stem directly from algorithmic choices explained here.



Title: NEON ATBD: NEON Imaging Spectrometer Level 1B Calibrated Radiance		Date: 03/25/2022
NEON Doc. #: NEON.DOC.001210	Author: W. Gallery	Revision: B

**2 RELATED DOCUMENTS AND ACRONYMS**

**2.1 Applicable Documents**

Applicable documents contain information that shall be applied in the current document. Examples are higher level requirements documents, standards, rules and regulations.

AD[01]	NEON.DOC.000001	NEON Observatory Design (NOD) Requirements
AD[02]	NEON.DOC.005003	NEON Scientific Data Products Catalog
AD[03]	NEON.DOC.005004	NEON Level 1-3 Data Products Catalog
AD[04]	NEON.DOC.005005	NEON Level 0 Data Product Catalog
AD[05]	NEON.DOC.000254	NEON Data Products Naming Convention (under revision)

**2.2 Reference Documents**

Reference documents contain information complementing, explaining, detailing, or otherwise supporting the information included in the current document.

RD[01]	NEON.DOC.000008	NEON Acronym List
RD[02]	NEON.DOC.000243	NEON Glossary of Terms
RD[03]	NEON.DOC.001207	NEON Imaging Spectrometer Geolocation Algorithm ATBD
RD[05]	NEON.DOC.015011	NEON AOP Concept of Operations
RD[06]	NEON.DOC.001517	NEON AOP Spectrometer Calibration Plan
RD[07]	NEON.DOC.(TBD)	NEON Imaging Spectrometer Level 1 Calibrated Radiance ICD
RD[08]	NEON.DOC.(TBD)	NEON Imaging Spectrometer Level 0 ICD

**2.3 External References**

External references contain information pertinent to this document, but are not NEON configuration-controlled. Examples include manuals, brochures, technical notes, and external websites.

ER [01]	
ER [02]	
ER [03]	

**2.4 Acronyms**

See Appendix A.



### 3 DATA PRODUCT DESCRIPTION

#### 3.1 Variables Reported

The data produced by this processing is listed in **Table 1**. See AD[05] for an explanation of the data products naming convention. In the product name, *dom* and *site* refer to the NEON domain and site respectively.

**Table 1.** Reported variables for data product NEON.*dom.site*.DP1.30005.

Variable	Units	Cross-reference (Ctrl+click to follow ref.)
Calibrated at sensor radiance	Watts m <sup>-2</sup> nm <sup>-1</sup> sr <sup>-1</sup> (TBR)	<a href="#">L(i, j, D)</a>
Radiance uncertainty	Watts m <sup>-2</sup> nm <sup>-1</sup> sr <sup>-1</sup> (TBR)	<a href="#">6.2 Reported Uncertainty</a>
Bad pixel mask (other, TBD)	(unitless)	<a href="#">bp(i, j)</a>

#### 3.2 Input Dependencies

The required inputs for this processing are listed in **Table 2**. A more complete description of the inputs, their origin and units is contained in RD[07], the NEON Imaging Spectrometer Level 1 Calibrated Radiance ICD.

**Table 2.** Input Dependencies.

Input	Reference	Description	Cross-reference (Ctrl+click to follow ref.)
NIS digital counts	RD[08]	Raw counts from science data stream	<a href="#">C(i, j, D)</a>
Laboratory flat field	RD[06]	Counts measured in lab viewing uniformly-illuminated source	<a href="#">f<sub>la</sub>(i, j)</a>
Radiometric calibration coefficients	RD[06]	Coefficients relating corrected counts to absolute radiance	<a href="#">d(i, j)</a> = dark count <a href="#">G(j)</a> = gain factor

#### 3.3 Product Instances

This algorithm produces the NEON data product NEON.*dom.site*.DP1.30005: calibrated at sensor radiance (see Section 3.1 Variables reported.)

#### 3.4 Temporal Resolution and Extent

The NIS radiance calibration algorithm is applied to each AOP flight line, which typically measure between 5 and 20 km in length and approximately 600 m in width. Flight speeds are typically around 100 knots (185.2 km/hour), and therefore, the time required to acquire flight lines of the lengths stated ranges from 1.6 to 6.5 minutes. The integration time for the NIS detector array is 100 milliseconds, so an image row is acquired every 100 milliseconds along-track.



### 3.5 Spatial Resolution and Extent

The NEON Imaging Spectrometer has an Instantaneous Field of View (IFOV) of 1.0 milliradians, which equates to ground sampling distance of 1 meter at a nominal flight of 1000 m above ground. The actual ground resolution varies with flight altitude and cross-track field-of-view.

Note that the calibrated spectral radiance discussed here does not constitute an “image.” Because the aircraft does not fly perfectly level or at a constant altitude, the data points projected on the ground do not lie on a regular grid. If displayed as an image, a straight line on the ground (e.g., a road) appears as a wavy line. This effect is exaggerated in **Figure 1** for which the aircraft was deliberately wobbled from side-to-side. The same data is shown in **Figure 2** after it has been georeferenced and regridded onto a uniform grid. Note that the wavy black pattern in **Figure 1** becomes the straight runway in **Figure 2**.

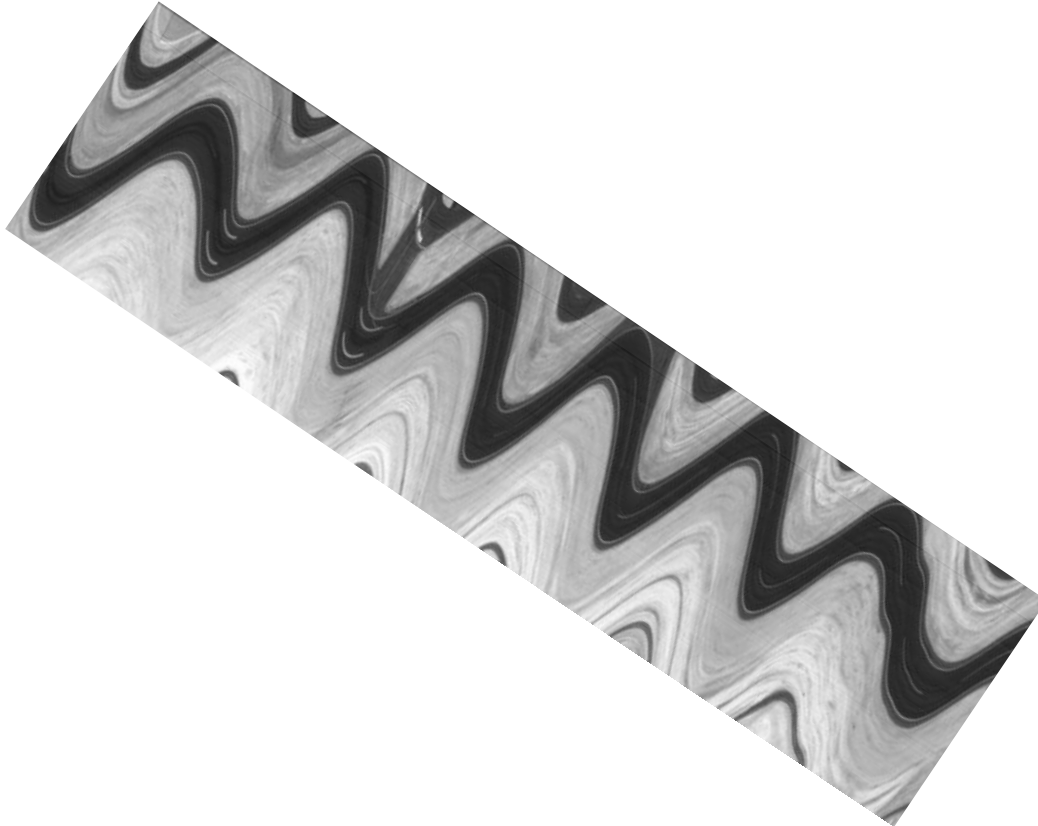


**Figure 1.** Un-geolocated radiance displayed as an image .

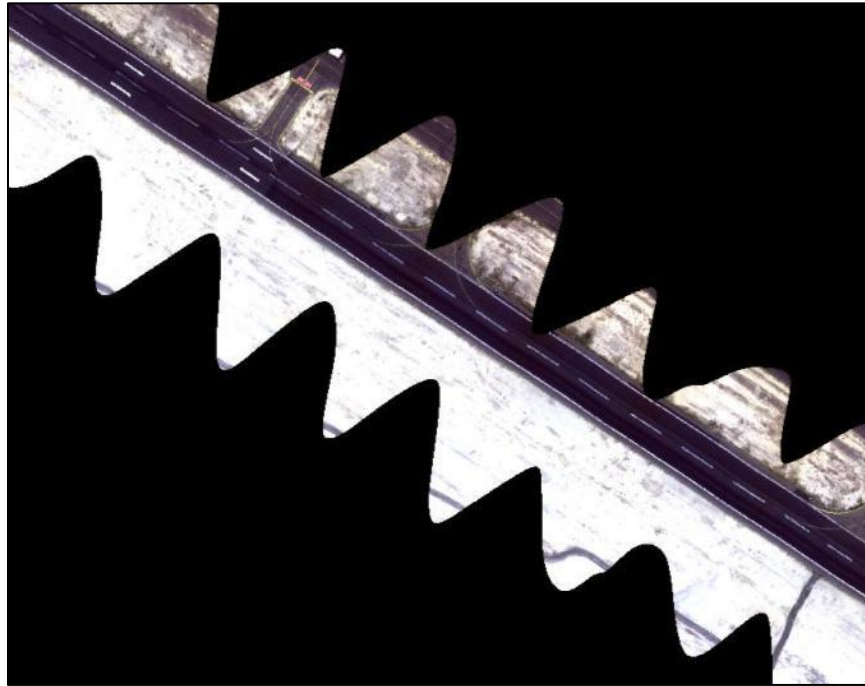


**Figure 2.** Geolocated and regridded radiance displayed as an image.



Title: NEON ATBD: NEON Imaging Spectrometer Level 1B Calibrated Radiance		Date: 03/25/2022
NEON Doc. #: NEON.DOC.001210	Author: W. Gallery	Revision: B

## 4 SCIENTIFIC CONTEXT

### 4.1 Theory of Measurement/Observation

#### 4.1.1 The NEON Imaging Spectrometer

The NEON Imaging Spectrometer (NIS) is the Next Generation (NG) version of the Airborne Visible/Imaging Infrared Spectrometer (AVIRIS) hyperspectral imager. AVIRIS instruments have been deployed on a broad range of measurement campaigns and are very successful in classifying vegetation, and surface mineralogy, and man-made features. A good description of the AVIRIS classic instrument and its applications is in *Green et al.*, 1998 and *Hamlin*, et al. 2010. The NIS is built by the AVIRIS group at the Jet Propulsion Lab (JPL). The first unit delivered to NEON was designated as the NEON Imaging Spectrometer Design Verification Unit (NISDVU) was flown in 2012. This instrument demonstrated the technical feasibility of the instrument concept. Subsequently, two operational instruments have been delivered to NEON - NIS-1 (delivered May 2013) and NIS02 (delivered in September 2013). The final instrument will be delivered to NEON in 4<sup>th</sup>-quarter 2014.

The NEON imaging spectrometer has the following specifications:

- Pushbroom sensor
- Focal plane: Teledyne TCM6604A
  - Mercury cadmium telluride (HgCdTe) detector
  - Spectral pixels: 480 rows total, ~428 rows used
  - Spatial: 640 total, ~598 used
  - Spectral range: 380 nm to 2510 nm
  - Spectral resolution: 6 nm FWHM, 5 nm sampling
- Total FOV: ~34 deg
- Spatial resolution at a nominal altitude of 1000 m: 1 m (1 mrad)

**Figure 3** shows a schematic diagram of the NIS spectrometer. In this figure, light enters through the slit and is diffracted off the grating surface in the first order then imaged onto the focal plane array surface. Rays shown in blue following the grating correspond to light at 380 nm, green rays correspond to light at 1350 nm, and red rays correspond to light at 2500 nm.

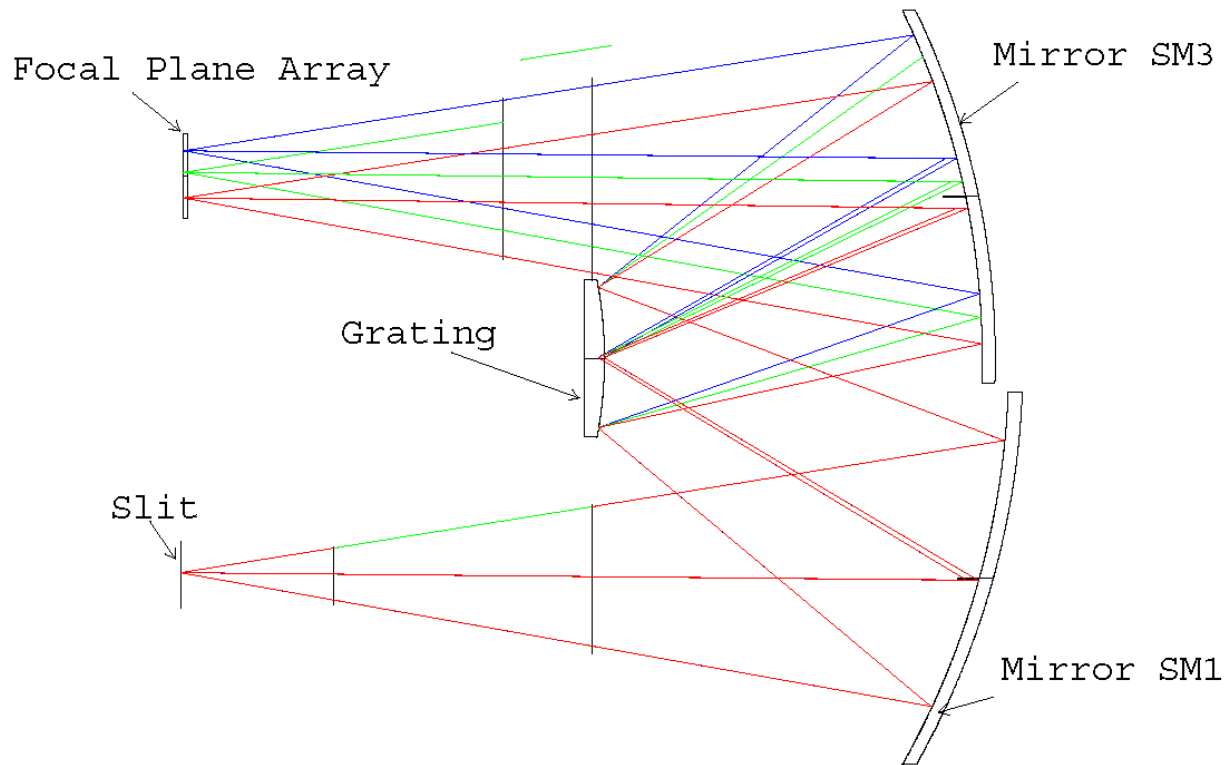


**Figure 3.** Optical ray trace through the NISDVU Spectrometer subsystem.

**Figure 4** is a picture of the Teledyne TCM6604A focal plane array (FPA) showing the spatial and spectral dimensions. The detector has 480 elements in the spectral direction (rows) and 640 elements in the spatial direction (columns). All 480- by 640-detector elements are read out, however several rows and columns around the outside boundaries of the focal plane are masked off to allow for determining the detector performance under no illumination (dark pedestal shift.) Integration time is 0.01 sec giving a data rate of 100 frames per second.

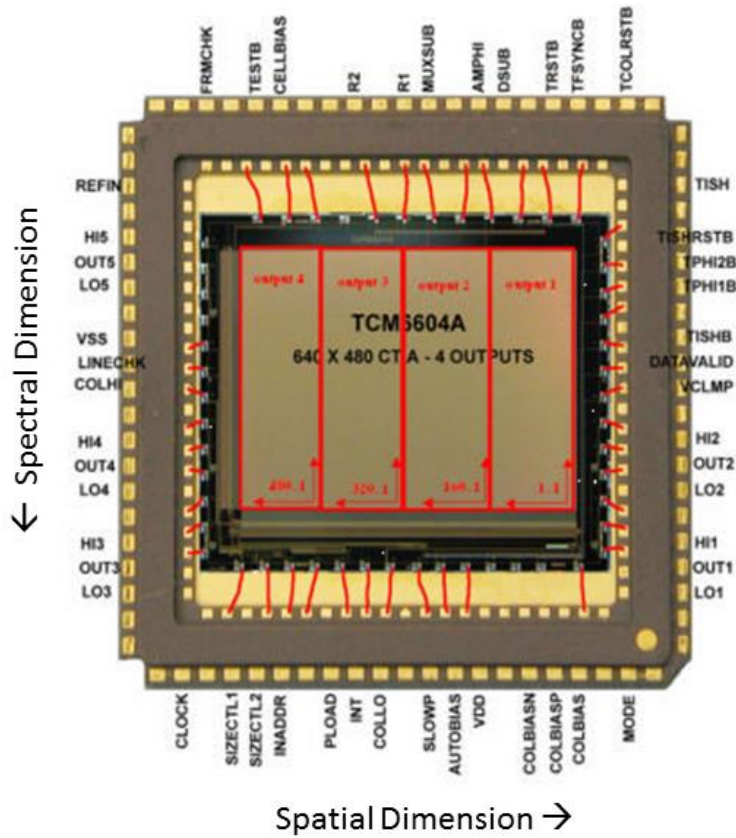
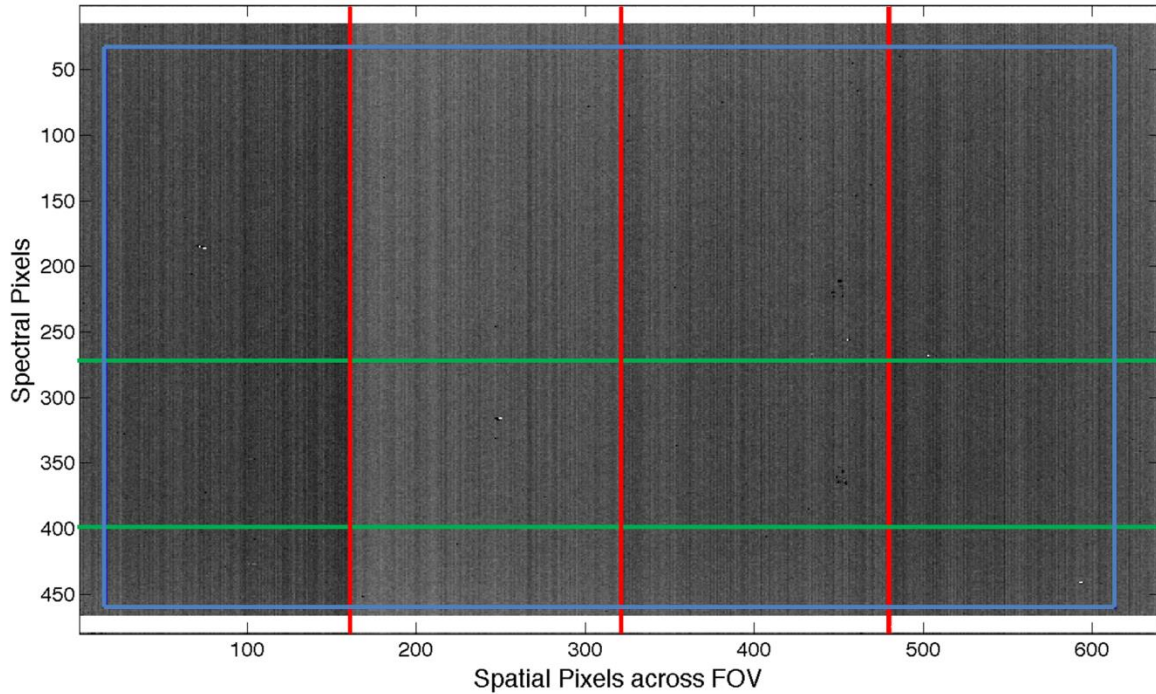


Figure 4. Annotated picture of the NIS focal plane (Ref. Hamlin et al. 2010).

Figure 5 shows an image from the detector while viewing a dark source (no illumination.) The various colored lines in the figure correspond to the following:

- The green horizontal lines show the order sorting boundaries
- The blue line encloses the area of the focal plane that provides valid data. The area outside the blue lines is physically masked off.
- The red vertical lines show the detector panel boundaries
- The white areas on the top and bottom of the image are used to determine the dark pedestal shift.



**Figure 5.** Image of the NIS focal plane dark-offset. The dark-offset is the detector output with no illumination of the focal plane.

In-flight calibration is performed using the shutter and the on-board calibrator (OBC). Viewing the closed shutter provides a dark source (no illumination). The OBC (a tungsten lamp) provides two levels of (non-uniform) illumination: medium and high. Finally, a red laser can also be projected into the field of view to monitor the spectral stability.

#### 4.1.2 Flight Operations

The operation of the NIS as part of the AOP is described in detail in reference RD[05] and shown in this [AOP Video](#). The following gives an overview of the flight measurement process.

**Figure 6** shows the flight path for a typical observation flight while **Figure 7** shows the flight lines (flight lines include only the periods when the NIS is taking data).



# High Park: 20130711A

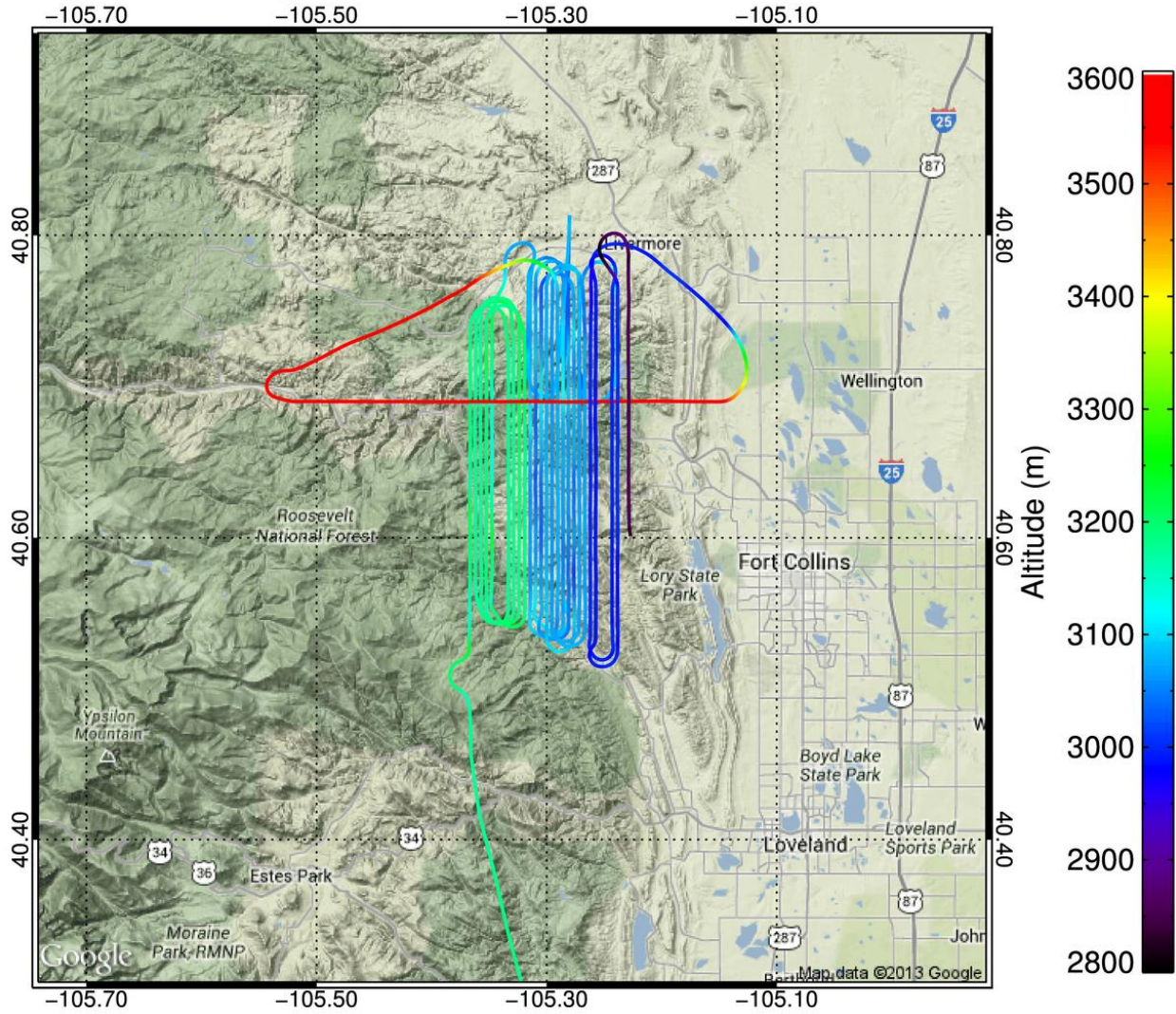


**Figure 6.** Flight path of the AOP flight over High Park, CO July 11, 2013. The color of the track indicates the altitude of the AOP above sea level.



# High Park 20130711A (from kml files)

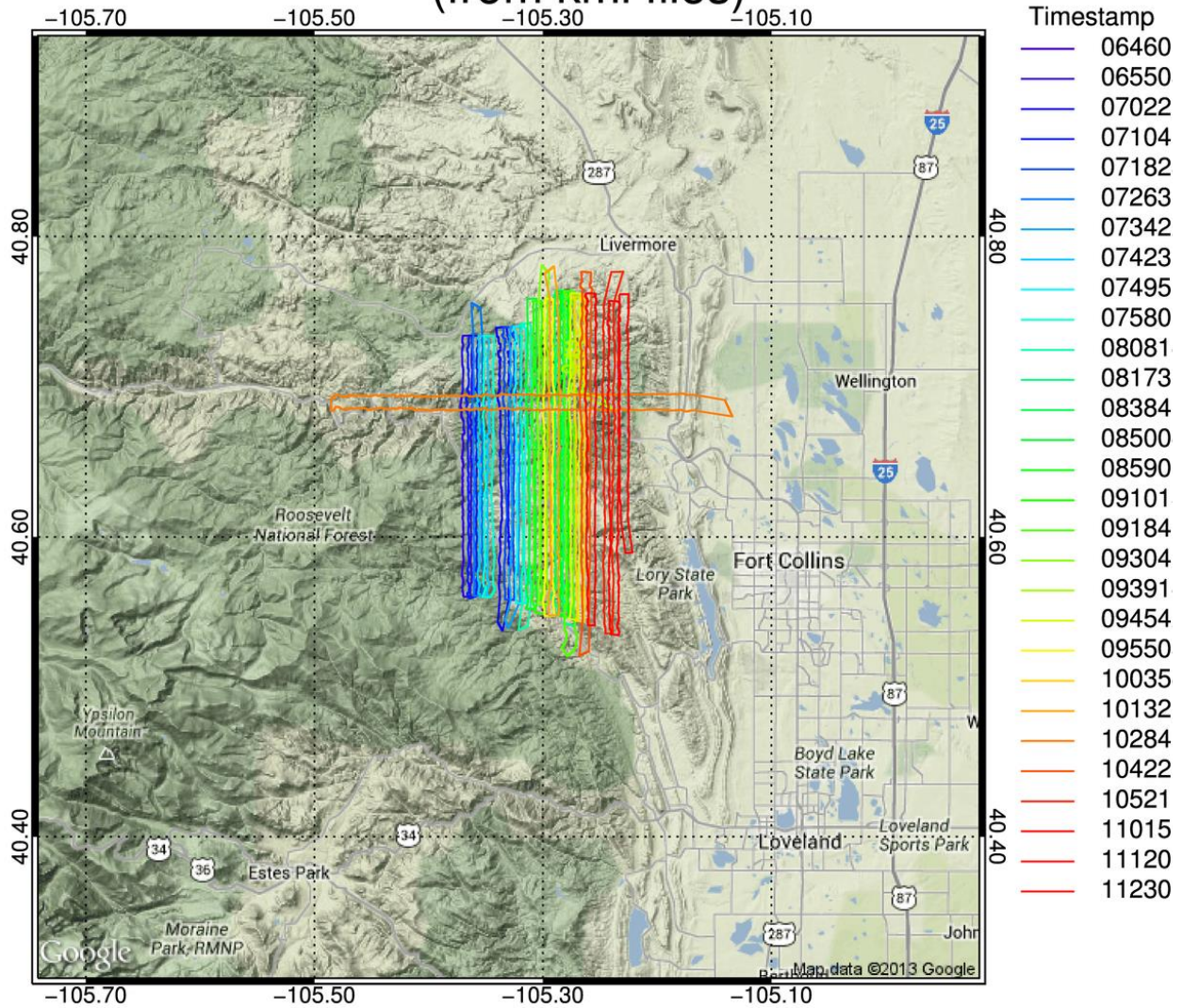


**Figure 7.** Outlines of the AOP flight tracks for July11, 2013. The different colors outline the individual flight tracks.

In a typical deployment, the NIS is operated as shown in **Table 3**. The number of lines viewing the target (ground) varies and is determined by the flight plan: 50,000 lines is typical but the number may vary from about 8000 to 100,000.



Title: NEON ATBD: NEON Imaging Spectrometer Level 1B Calibrated Radiance		Date: 03/25/2022
NEON Doc. #: NEON.DOC.001210	Author: W. Gallery	Revision: B

**Table 3.** NIS operating sequence during a typical flight.

Flight Leg	NIS status	Spatial lines
Fly from forward operating base (FBO) to survey area	NIS not recording	
Conduct flight line	Observe: OBC-mid-level (short sequence) OBC-high-level (short-sequence) OBC dark shutter Target OBC dark shutter ( $\overline{Dark}$ ) OBC mid-level source ( $\overline{OBC}_{mid}$ ) OBC high-level source ( $\overline{OBC}_{high}$ ) OBC red laser	Not recorded Not recorded 1000 variable, 50000 typical 1000 1000 1000 1000
Turn around for next flight line	NIS not recording	Not recording
Conduct next flight line	...	...
Conduct next flight line	...	...
Return to FOB	NIS not recording	

The data for each flight line are stored and calibrated separately.

#### 4.2 Theory of Algorithm

Calibration of the spectrometer data consists of three phases:

1. **Calibrating the spectrometer.** In this phase, the spectrometer measures well-characterized radiance sources in the laboratory. These measurements generate data required to calculate absolute radiance from the raw spectrometer output (digital counts). This phase is conducted at periodic intervals to ensure the stability of the calibration.
2. **Calibrating the science data.** In this phase, the raw data from in-flight measurements is converted to absolute radiance using the results of the laboratory calibration. This calibration includes:  
 dead/bad pixel determination  
 dark pedestal shift correction  
 electronic ghost correction  
 radiometric calibration
3. **Vicarious Calibration:** the spectrometer calibration is verified by a program of vicarious calibration. The AOP measures spectra over well-characterized, homogenous stable ground sites. Comparison between the AOP measured spectra and the known spectra of the sites verifies the laboratory calibration.

These steps are described in more detail in the following sections.



#### 4.2.1 Laboratory Calibration

This section presents a simplified version of the laboratory calibration process. It is described in detail in the NEON Technical Memo RD[04]

Assume that the output of an ideal linear detector in response to the incident radiance obeys the following linear equation:

$$L(i, j, l) = a(i, j)[C(i, j, l) - d(i, j)] \quad 1.$$

where:

$i$  = column index (spatial dimension) of the focal plane: dimension =  $n_c$

$j$  = row index (spectral dimension) of the focal plane: dimension =  $n_r$

$l$  = index of the incident radiance  $L$  level: dimension = 3: 0 = dark, 1 = mid-level, 2 = high-level (in practice,  $l = 2$  is not used)

$C(i, j, l)$  = detector output, in counts

$L(i, j, l)$  = incident radiance, in watts  $m^{-2} nm^{-1} sr^{-1}$

$a(i, j)$  = radiometric coefficient, in watts  $m^{-2} nm^{-1} sr^{-1} count^{-1}$

$d(i, j)$  = dark count (spectrometer output at zero incident radiance), in counts

The detector output  $C(i, j, l)$  is measured at two levels of incident radiance:  $L(i, j, 0) = 0$  and  $L(i, j, 1)$ . The calibration coefficients  $a(i, j)$  and  $d(i, j)$  from eq. 1:

$$\begin{aligned} d(i, j) &= C(i, j, 0) \\ a(i, j) &= L(i, j, 1) / [C(i, j, 1) - C(i, j, 0)] \end{aligned} \quad 2.$$

In the laboratory, the incident radiance  $L(i, j, l)$  is generated by an integrating sphere whose illumination is assumed spatially homogenous. A transfer radiometer, including a NIST-traceable source, provides the absolute calibration.

It is convenient to separate out the spatial and spectral variations in  $a(i, j)$  by factoring  $a(i, j)$  into two other terms:

$$a(i, j) = G(j) * f_{lab}(i, j) \quad 3.$$

where:

$G(j)$  = spectral gain factor: dependent only on the wavelength, units of watts  $m^{-2} nm^{-1} sr^{-1} count^{-1}$



$f_{lab}(i, j)$  = flat field response: unit less

with the constraint that:

$$mean(f_{lab}(i, j)) = 1 \tag{4}$$

When viewing a spatially uniform source,  $f_{lab}(i, j)$  measures spatial variations in detector response, hence the name “flat field response”. Combining equations 3 and 4 gives:

$$\begin{aligned} G(j) &= mean_i(a(i, j)) \\ f_{lab}(i, j) &= a(i, j)/G(j) \end{aligned} \tag{5}$$

Eq. 1 can now be written as

$$L(i, j, \lambda) = G(j)f_{lab}(i, j)[C(i, j, \lambda) - d(i, j)] \tag{6}$$

**Figure 8** and **Figure 9** show plots of values of  $f_{lab}(i, j)$  for the NISDVU. The features at spectral rows 273 and 399 correspond to the order sorting filter boundaries. **Figure 10** shows the gain function  $G(j)$

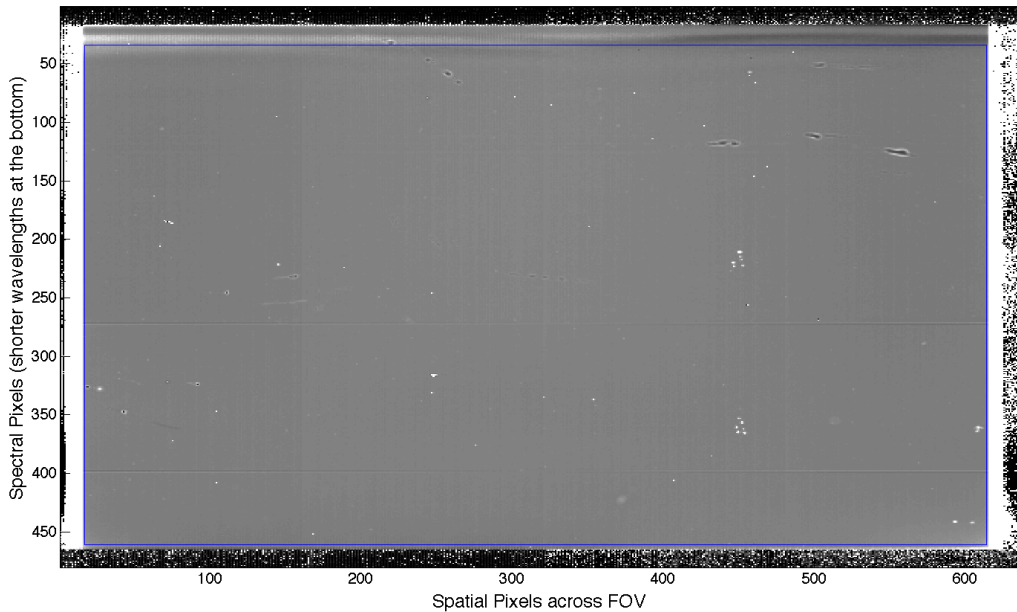


**Figure 8.** Image plot of the flat field  $ff(i, j)$  for NISDVU.

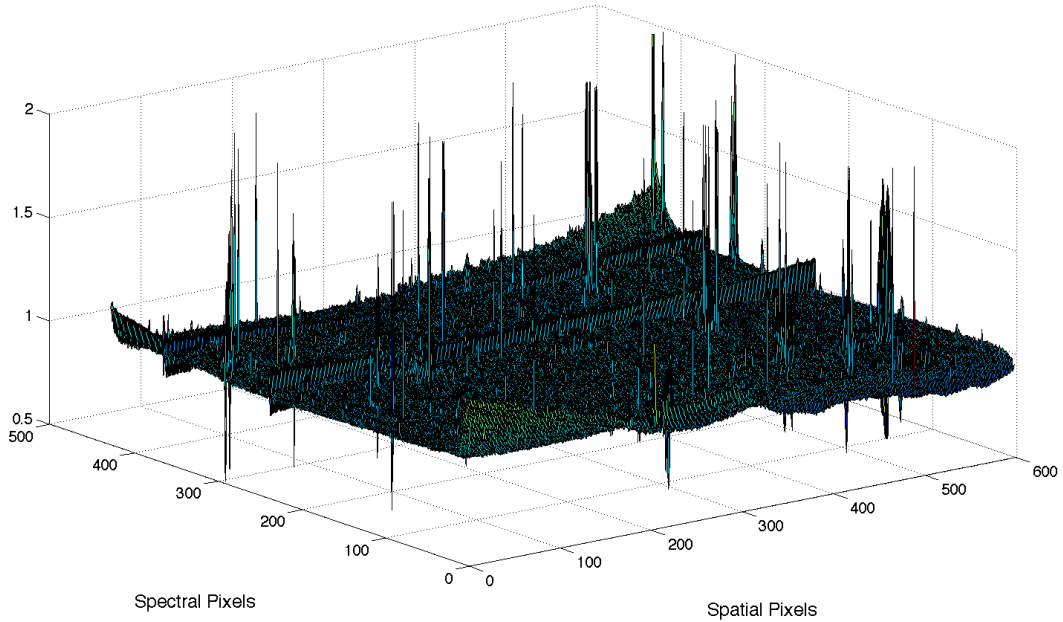


**Figure 9.** Surface plot of the flat field  $ff(i,j)$  for NISDVU extending the radiometric calibration coefficients to the entire Focal Plane Array (FPA). Spikes are indicative of poor or dead pixels. The extended sharp features at spectral pixels 273 and 399 result from order-sorting filters applied to the FPA.

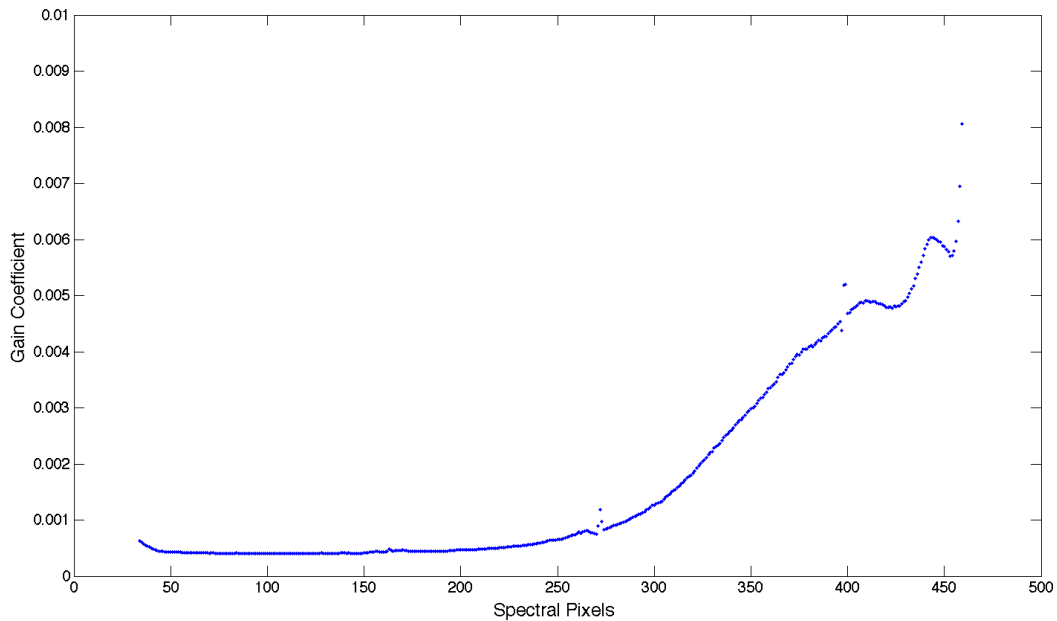


**Figure 10.** Plot of the gain function  $G(s)$  for NISDVU.



Title: NEON ATBD: NEON Imaging Spectrometer Level 1B Calibrated Radiance		Date: 03/25/2022
NEON Doc. #: NEON.DOC.001210	Author: W. Gallery	Revision: B

The description above applies to an ideal instrument. Experience with the Teledyne TCM6604A detector indicates that the spectrometer counts  $C(i, j, 1)$  and the dark count  $d(i, j)$  must be corrected for effects characteristic of this chip. These effects include dead pixels, dark pedestal shift, and electronic panel ghost. To include these effects, eq. 6 must now be written as:

$$L(i, j, l) = G(j) f_{lab}(i, j) f_{OBC}(i, j) [C(i, j, k) - d(i, j) - p(l) - g(i, j)] \quad 7.$$

where:

$f_{OBC}(i, j)$  = the OBC flat field

$p(l)$  = dark pedestal shift

$g(i, j)$  = electronic panel ghost.

These effects are characterized as part of the laboratory calibration and are discussed in detail in RD[06]. The following section describes the application of the laboratory calibration results to the science data collected in the field.

#### 4.2.2 Science Data Calibration

The overall calibration process is shown in **Figure 11**. The following sections describe the individual steps in the process.

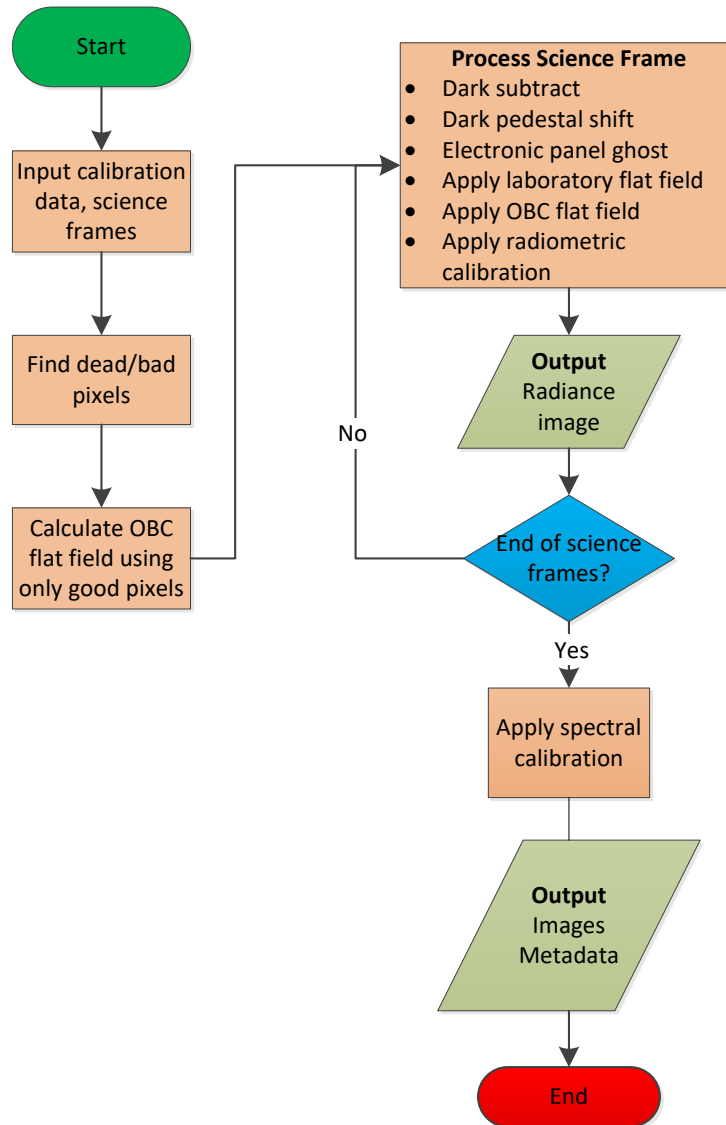


Figure 11. Spectrometer data processing flowchart.



The science data calibration process must account for several characteristics of the detector:

- **Dead/bad/blinking pixels:** some of the focal plane pixels are either dead (have no response), bad (out-of-range response) or blinking (temporally varying response). These pixels are flagged and identified in the Bad Pixel Map (Ref.: Section 4.2.2.1) that is generated as part of this procedure.
- **Dark pedestal shift:** illumination anywhere in the focal plane causes a shift in the dark count everywhere on the focal plane.
- **Electric panel shift:** illumination in any of the four panels of the focal plane causes a “ghost” image to appear in the other three panels. Laboratory measurements show that the ghost image is 0.15% or more of the original image.

The first of these effects is characterized using the data from the OBC taken at the end of each flight line and are applied to uniformly to all the science data in that flight line. The last two are applied separately to each science frame in the flight line.

The following sections describe each of these processes.

#### 4.2.2.1 Dead/Bad/Blinking Pixels

Pixels are considered “dead” or “bad” if their response falls outside of a certain range. These pixels must be identified and flagged. The bad pixels are identified from a flat field generated from the OBC measurements taken at the end of each flight line. They are identified from the OBC measurements rather than the laboratory calibration because some of them are transient (blinkers) and may not show up in the laboratory.

As shown in **Table 3**, at the end of each flight line, the spectrometer views the OBC dark field, mid-level source and the high-level source. An OBC flat field is generated from the difference in the raw counts between the OBC dark field and the mid-level source (currently, the high-level source data is not used.) The bad pixels are identified from this flat field.

The first step in this process is to calculate the response  $R(i, j)$  to the OBC mid-level source after correcting for the OBC dark source and the laboratory flat field. This response is defined in eq. 8 and is shown in **Figure 12**.

$$R(i, j) = f_{Lab}(i, j)[C(i, j, 1) - C(i, j, 0)] \quad 8$$

where  $C(i, j, l)$  is now the measured counts obtained by viewing the OBC dark source ( $l = 0$ ) and mid-level source ( $l = 1$ ).



The details of calculating the bad pixel mask and the OBC flat field from  $R(i, j)$  are given in the flow chart shown in **Figure 13**. The results of applying the different steps are shown in **Figure 14** through **Figure 16**. The result of this process is the OBC flat field  $f_{OBC}(i, j)$  (which includes the bad pixel mask.)

The smoothing process and the parameters used here are based on previous experience gained from the AVIRIS next-gen sensor and are subject to change.

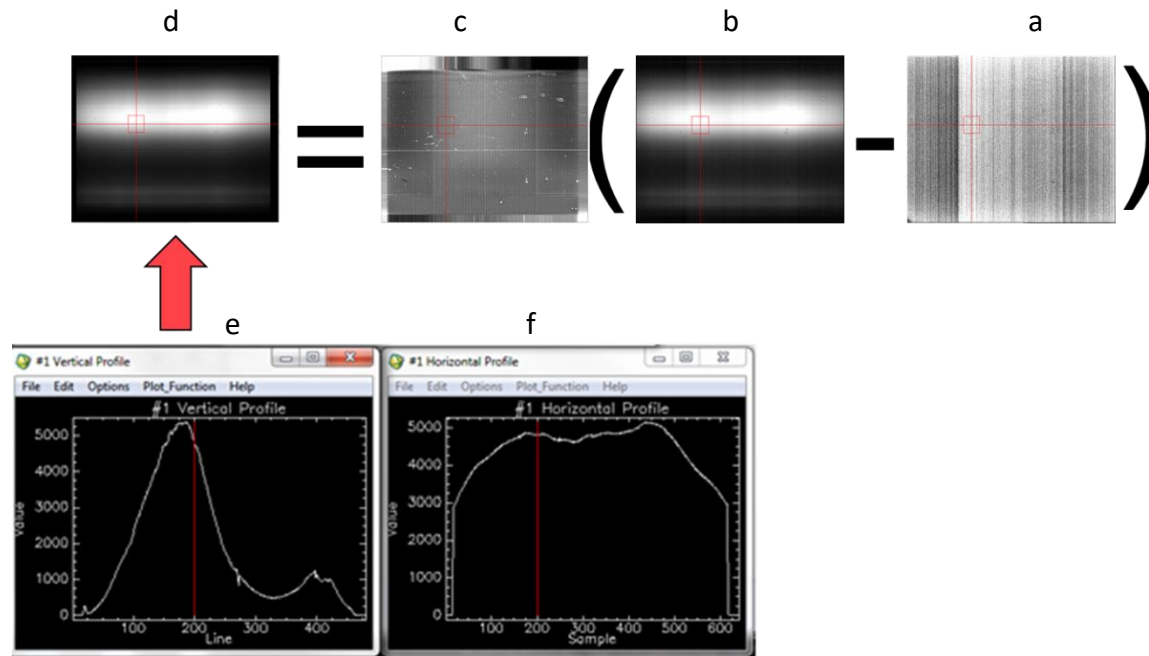


**Figure 12.** The corrected response  $R(i, j)$  to the OBC mid-level source: a. dark response, b. mid-level bright source, c. laboratory flat field, d. corrected response, e. spectral cross-section through d, f. spatial cross-section through d.

Note: in these and subsequent images, the horizontal axis (columns) represents the spatial dimension

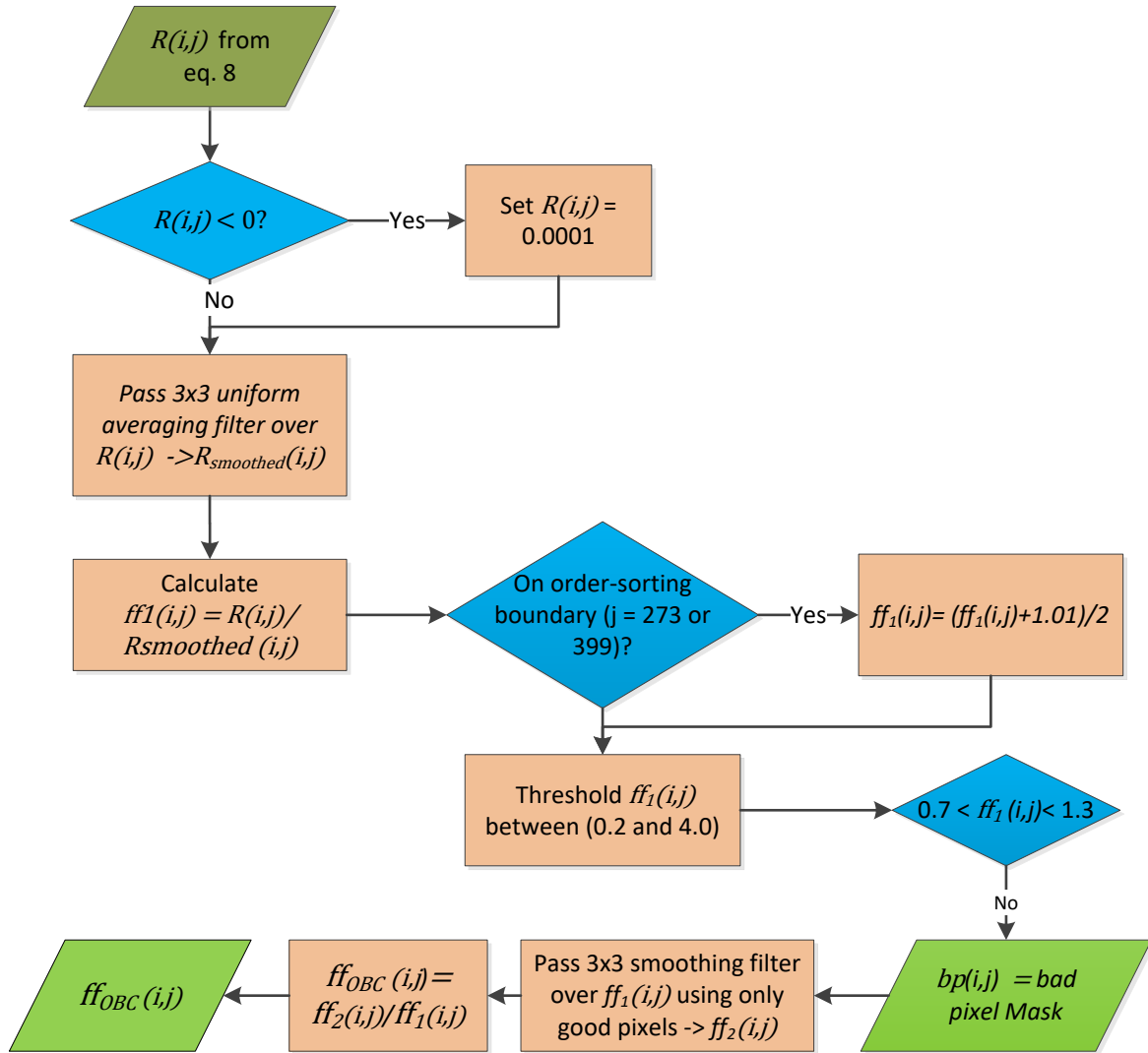
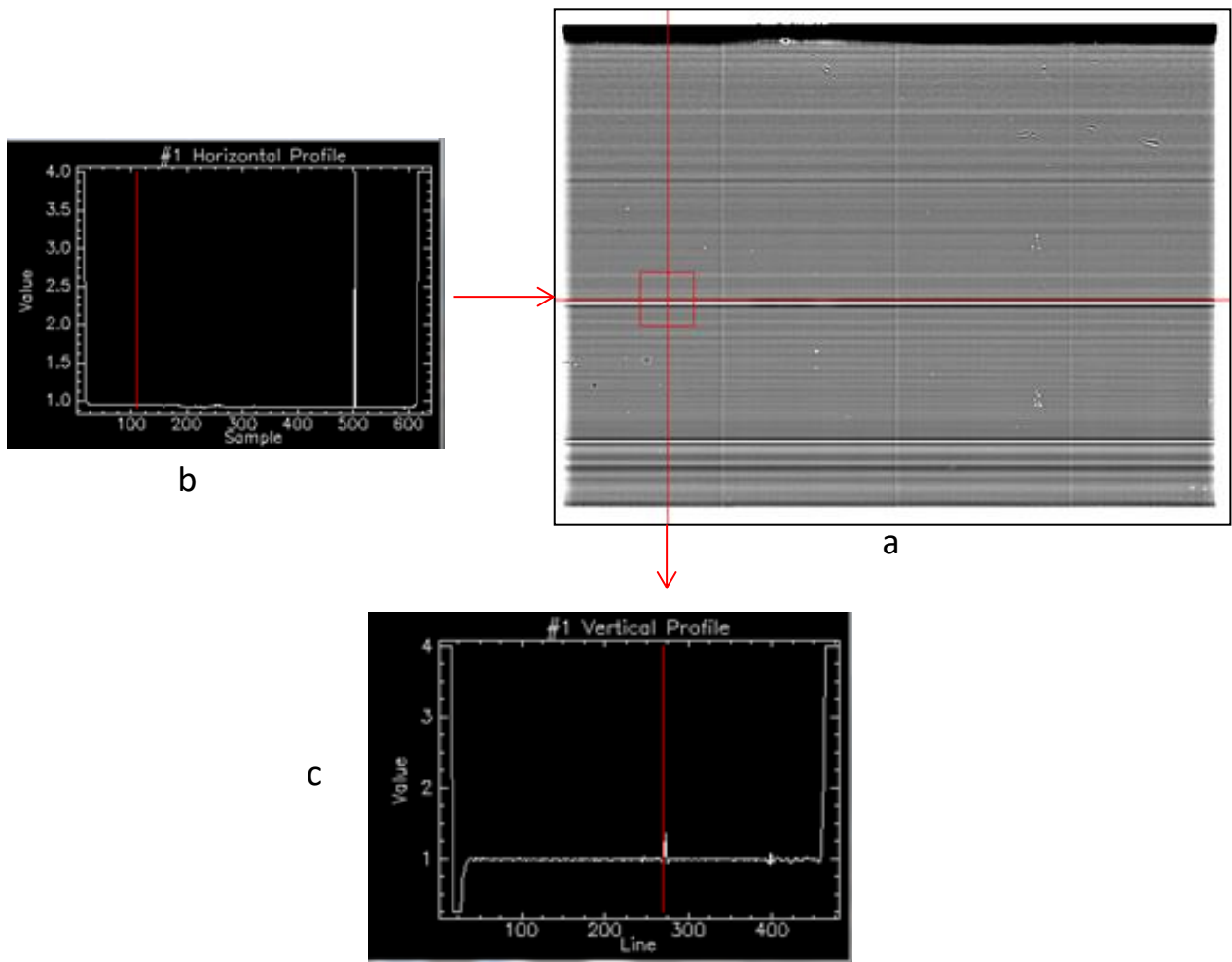
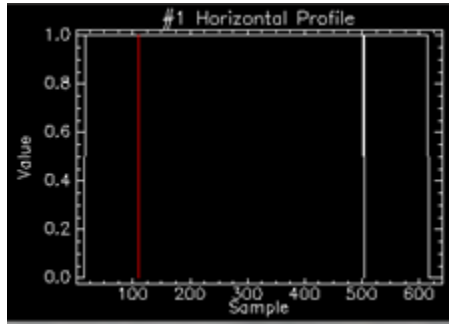


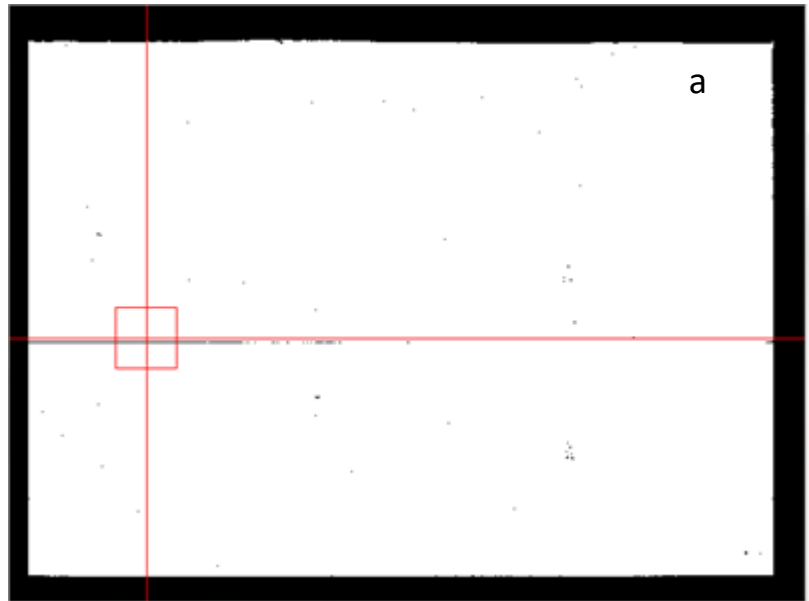
Figure 13. Flow chart showing the calculation of the OBC bad pixel mask and flat field.



**Figure 14.** The preliminary OBC flat field  $ff_1$ : a. preliminary flat field, b. spatial cross section through a, c. spectral cross-section through a.



b



c

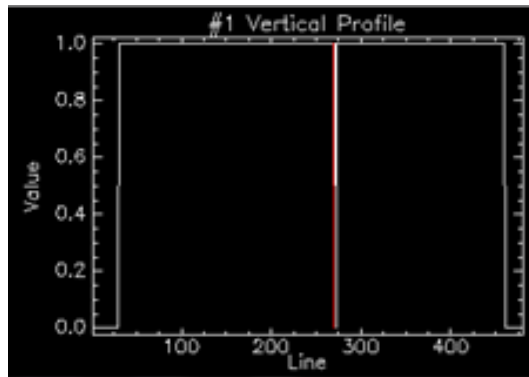


**Figure 15.** The OBCbad pixel mask: a. OBC flat field, b. spatial cross-section through a., c. spectral cross-section through a.

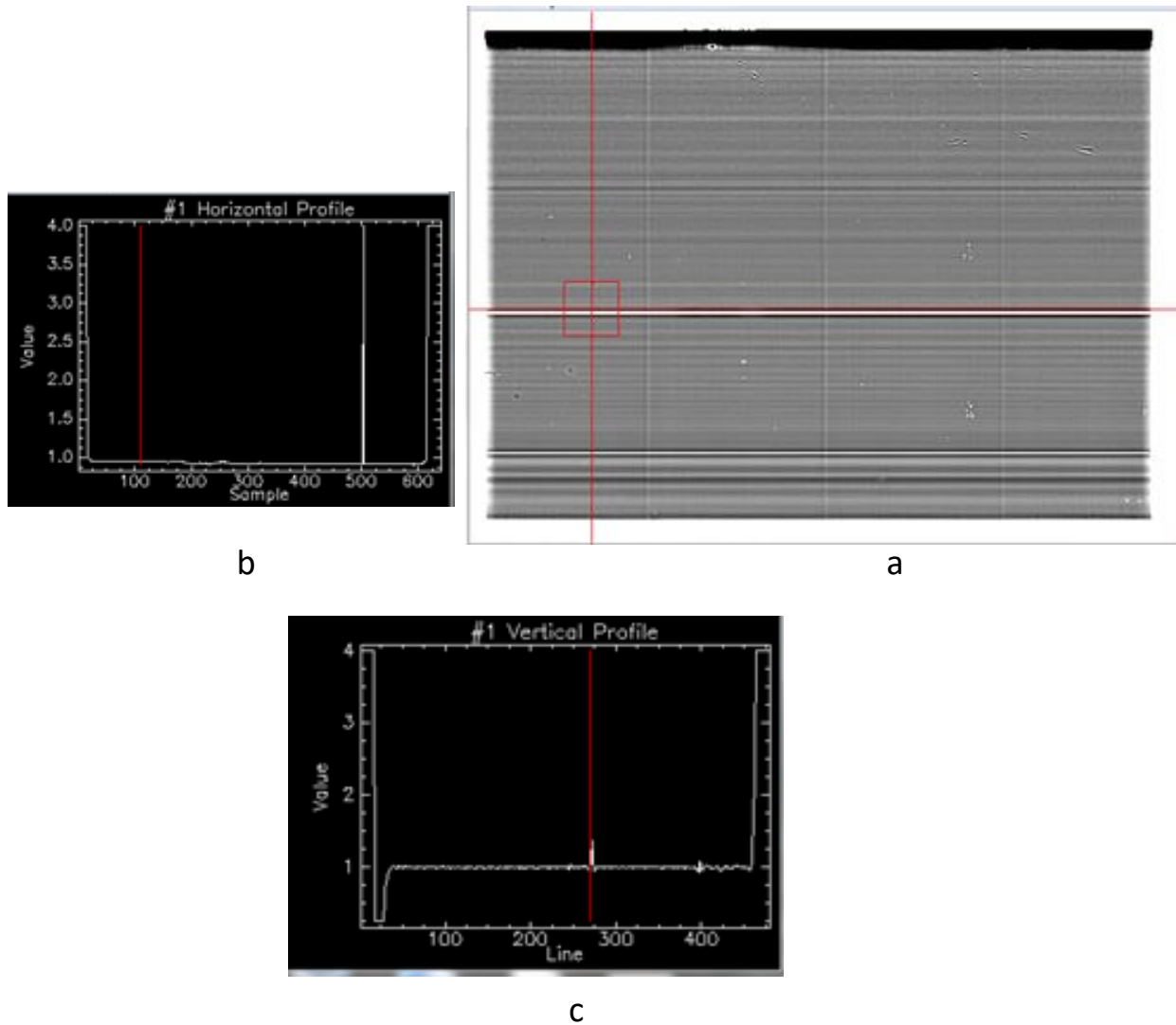


**Figure 16.** OBC flat field with bad pixels removed: a. OBC flat field, b. spatial cross-section through a., c. spectral cross-section through a.

#### 4.2.2.2 Dark Pedestal Shift

Every time the FPA is illuminated, the entire image is shifted by a fixed amount relative to dark values. The amount of this shift is found by averaging the counts in the regions in the science frame that are not illuminated. The non-illuminated regions are the physically masked over margins of the focal plane detector array. This average is called the dark pedestal shift and is indicated by  $p(i)$ . The index  $i$  here indicates the frame number of the science data.

**Figure 17** shows an image (in counts) of the OBC dark calibration target. The blue areas at the top and bottom of the image indicate the regions of the focal plane that are masked and therefore receive no light. (There is a similar masked area at the right and left margins that is not shown.) **Figure 17b** shows an image of the OBC mid calibration target. Note that the masked area is nearly black, indicating low



signal. **Figure 17c** shows the raw signal (in counts) in the masked area at the top and bottom of the image averaged over row. Ideally, the dark values in **Figure 17c** would be zero since these pixels are not illuminated. However, due to the dark pedestal offset introduced by the focal plane technology, the readout on dark regions becomes negative when the focal plane is illuminated. This negative value is dependent upon the illumination of the entire illuminated focal plane, and therefore must be subtracted on a frame-by-frame basis. In the current version of the algorithm the average of the 640-value vector in **Figure 17c** is averaged, and subtracted from each value in the frame.

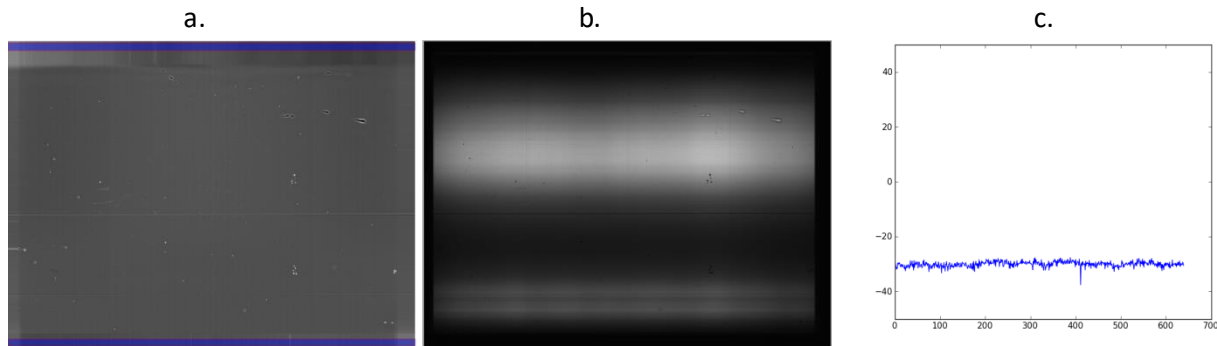


**Figure 17.** Dark pedestal shift: a. OBC dark calibration image, b. OBC mid-calibration image, c. the dark pedestal shift averaged over rows for the image in b.

#### 4.2.2.3 Electric Panel Ghost

The detector focal plane is divided into four panels (see **Figure 4**). When an image is displayed in one of the four panels, a ghost appears in each of the other three panels. This ghost is about 0.15% of the image in the other panel. To correct for this effect, 0.15% of the counts in panel 1 are subtracted from each of panels 2, 3 and 4, then 0.15% of panel 2 is subtracted from panels 1, 3 and 4, and so on. Since the magnitude of the subtracted amount (0.15% of the signal) is very small, the order of subtraction is not significant. The subtracted amount is indicated by  $gh(i, j, l)$ .

**Figure 18** illustrates this phenomenon. Here a bright image in the leftmost panel is seen as a ghost in the other panels to the right that are not illuminated.

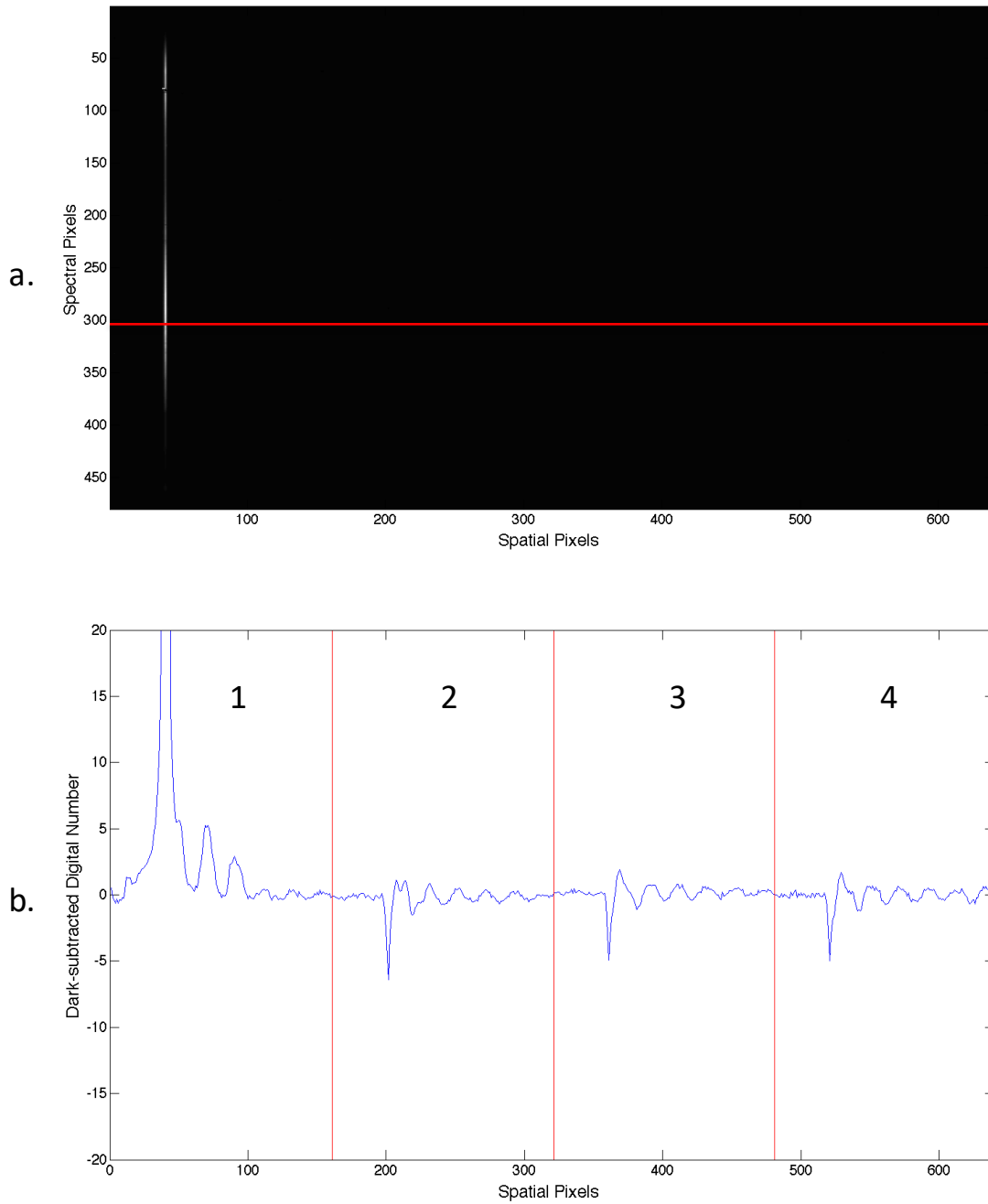


**Figure 18.** Electric panel ghost: a. FPA frame showing expected illumination in area 1, b. horizontal cross section at the red line (line 300 of frame in a.) The red vertical lines in b delineate separate detector areas. A negative ghost is present in areas 2, 3, and 4 from the illumination in area 1.



#### 4.2.2.4 Radiometric Calibration

Following Eq. 7, the radiometric calibration of the science data is performed using the following two equations:

$$C_{corr}(i, j, l) = C(i, j, l) - c(i, j) - p(i, j) - g(i, j, l) \quad 9.$$

$$L(i, j, l) = G(j) * f_{OBC}(i, j) * f_{lab}(i, j) * C_{corr}(i, j, l) \quad 10.$$

where the index  $l$  indexes the science data frame.

#### 4.2.2.5 Spectral Calibration

The spectral calibration of the imaging spectrometer consists of two parameters describing the position and width of the spectral response functions (SRF) for a given pixel. The band-center of the SRF is found using well-known emission lines illuminating the full spatial FOV and different spectral areas of the focal plane at the same time as shown in **Figure 19**.

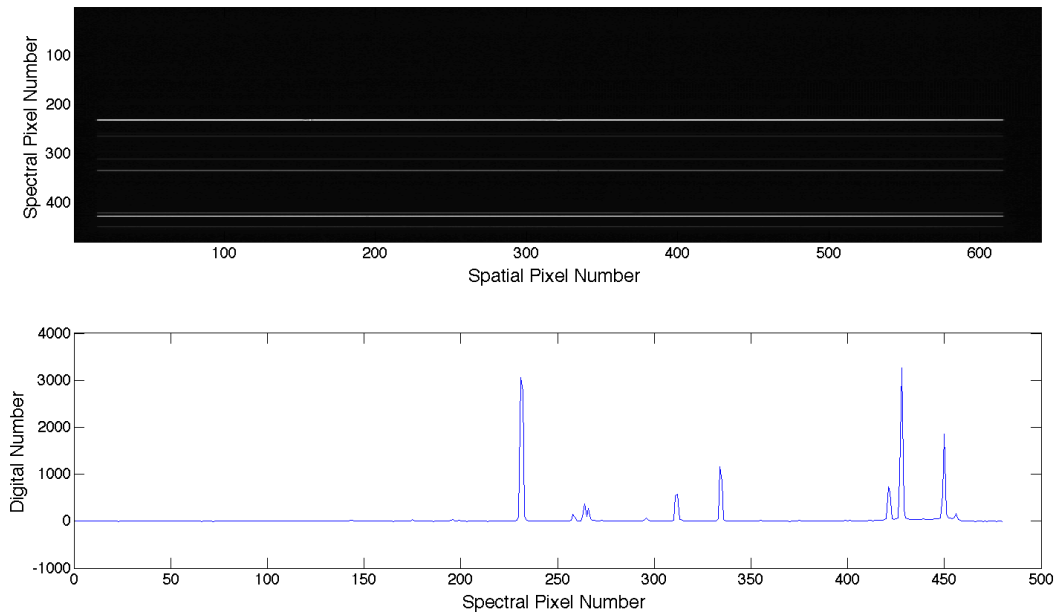


**Figure 19.** Spectral calibration of band centers: a. FPA frame with Hg area-lamp illuminating various spectral channels, b. Spectral trace along spatial column 300.

The pixels near the illuminated area are fit with a Gaussian curve to determine the center spectral pixel number for each emission line. **Figure 20** shows the spectral pixel number vs wavelength for each emission line. The figure shows an excellent linear fit of the pixel number to wavelength. This spectral linearity is then exploited to extend the calibration to the remaining spectral pixels.

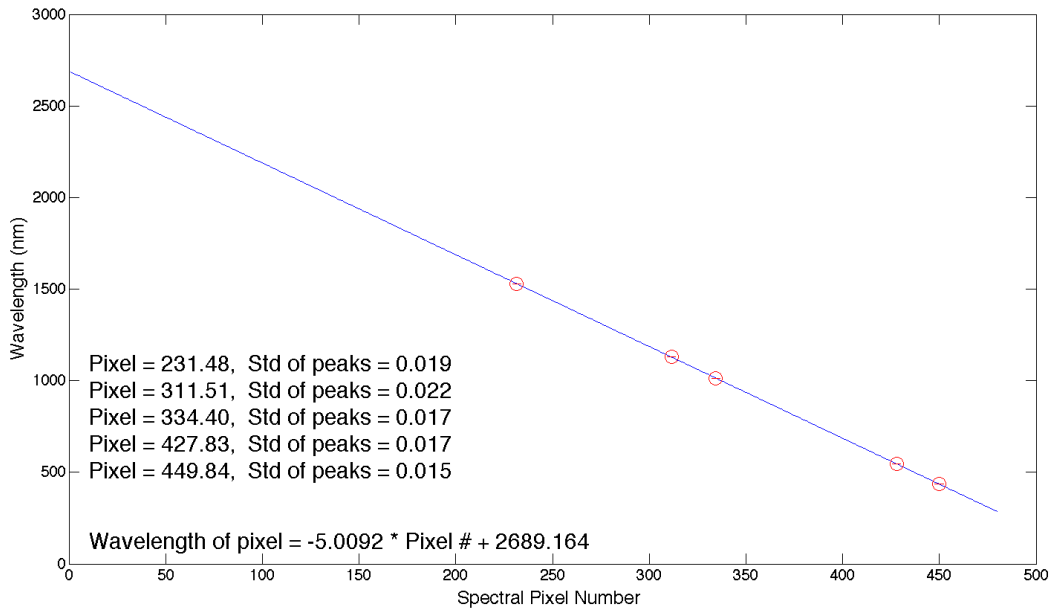


Figure 20. Spectral pixel number vs wavelength.

The width of the spectral response function (SRF) at the 50% point is known as the Full-Width at Half Maximum (FWHM). This is illustrated in **Figure 21**. A measure of the FWHM over the full spatial and spectral extent of the provides a measure of the uniformity of the instrument response. The spectral FWHM for NISDVU for one spatial position (focal plane column) is shown in **Figure 22**. The spectral resolution requirement for the NIS is that the FWHM  $\leq 10$  nm. **Figure 22** shows that this requirement is met over the full spectral range.

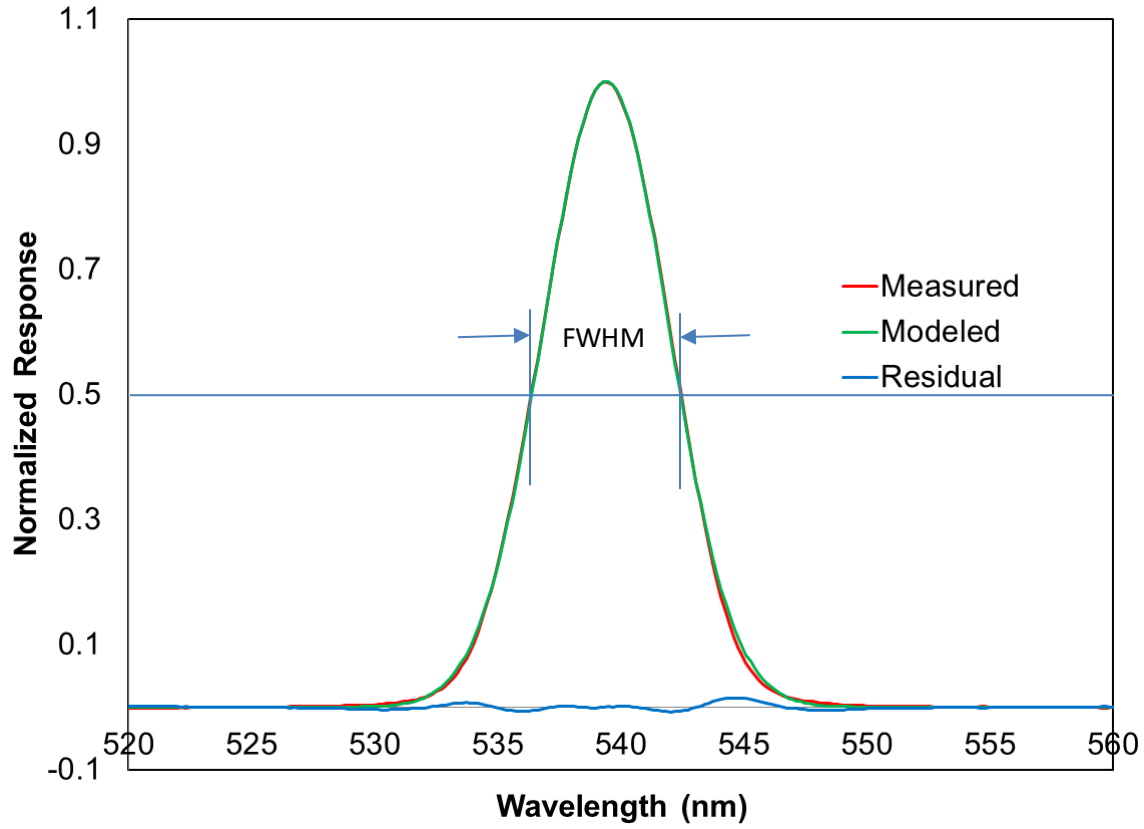


Figure 21. Normalized SRF for a single pixel compared to a modeled Gaussian SRF.

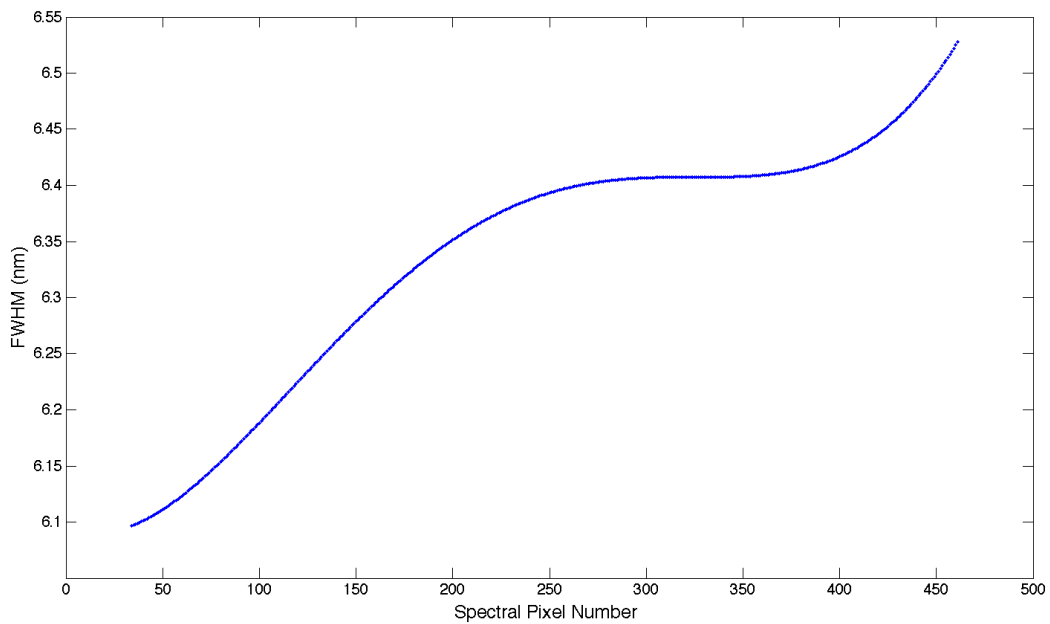


Figure 22. FWHM of SRF through the spectral channels of the FPA.



Title: NEON ATBD: NEON Imaging Spectrometer Level 1B Calibrated Radiance		Date: 03/25/2022
NEON Doc. #: NEON.DOC.001210	Author: W. Gallery	Revision: B

**5 ALGORITHM IMPLEMENTATION**

This section describes the steps used to process the raw spectrometer counts to absolutely calibrated radiance. Some of the steps and numerical parameters, specifically the smoothing and thresholding steps, were developed by JPL based on their experience and are somewhat ad hoc. As we gain more experience with the data ourselves, these steps will be reviewed and possibly changed.

The source of the input data is described in detail in the Interface Control Document (ICD) for this process (RD[07]).

**5.1 Processing Steps**

The spectrometer data stream consists of a number of data frames beginning with the OBC data recorded at the beginning of the flight line and ending with the OBC data recorded at the end. Each data frame is a 640 by 480 array of numbers from the focal plane array as shown in **Figure 4**. (Note: the convention used here is that arrays are read in column order, i.e., row by row). Frames are recorded at 100 frames per second. The first row of each frame contains metadata, the following 479 rows contain the data.

Row one of each frame contains the information shown in **Table 4**.

**Table 4.** Contents of row one of the frame data.

Bytes	Data	Format	Comments
0-7	Unused	I16	NGISWindows epoch time with initial JPL NGIS operating system
8-11	GPS seconds	32-bit integer	NGIS operating system sets these to zero
12-15	Unused		
16-17	FPIE timestamp	16-bit integer	100 μsec since GPS pulse per second
18-639	Unused		
640-1279	OBC state information	(TBD)	2 = OBC dark offset 3 = Science data 4 = OBC dark offset 5 = Mid OBC data 6 = Bright OBC data 7 = OBC Laser data
Note: Time = GPS_Seconds + (FPIE_timestamp x 100.0e-6) (FPIE: focal plane electronics interface)			

Each subsequent row of data contains 640 2-byte integers comprising the spatial data for one wavelength band. However, only bytes 17 through 614 contain usable data (see **Table 5**).



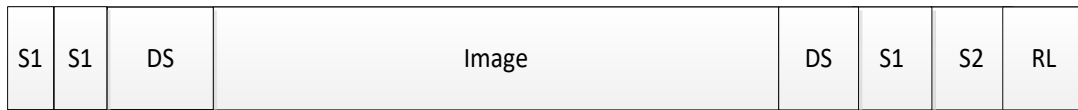
Title: NEON ATBD: NEON Imaging Spectrometer Level 1B Calibrated Radiance		Date: 03/25/2022
NEON Doc. #: NEON.DOC.001210	Author: W. Gallery	Revision: B

**Table 5.** Specifications of a row of frame data.

Words (two-byte signed integer)	Content	Comments
1-16	NA	not illuminated
17 to 614	data	spatial data
615 to 640	NA	not illuminated

For the dark pedestal shift, the rows 2 through 14 and 467 through 479 are used.

The sequence of the spectrometer data for a flight line is sketched in **Figure 23**. The nominal number of frames in each block is listed in **Table 3**.



DS = dark source  
 Image = radiance image  
 S1 = source 1  
 S2 = source 2  
 RL = red laser

**Figure 23.** Sequence of the raw data for one flight line.

The following equations use the same notation introduced in eq. 1

**Step 1. Process the OBC data to the flat field and bad pixel mask**

**Inputs:**

- Laboratory flat field  $ff_{lab}(i, j)$
- The raw science data  $C(i, j, l)$  from observation of the OBC's at the end of the flight line.

**Outputs:**

- The OBC flat field  $ff_{OBC}(i, j)$
- The OBC dark count  $dc_{OBC}(i, j)$
- The bad pixel mask  $bp(i, j)$

**Process:**

1. Average the raw counts  $C(i, j, l)$  over the frames corresponding to DS and S1 in **Figure 22**:  
 $C_0(i, j) = \text{ave}(C(i, j, l) \text{ over } l \text{ in DS at end of the flight line})$   
 $C_1(i, j) = \text{ave}(C(i, j, l) \text{ over } l \text{ in S1 at end of the flight line})$
2. Calculate the OBC response  $R(i, j)$  given in eq. 8:  

$$R(i, j) = f_{lab}(i, j)[C_1(i, j) - C_0(i, j)]$$
3. For each pixel, if  $R(i, j) < 0$ , set  $R(i, j) = 0.0001$



4. Pass a 3 by 3 uniform averaging filter over  $R(i, j)$  to get  $R_{\text{smoothed}}(i, j)$

$$R_{\text{smoothed}}(i, j) = \left( \sum_{u=i-1}^{i+1} \sum_{v=j-1}^{j+1} R(u, v) \right) / 9$$

5. Calculate the preliminary flat field  $ff_1$

$$ff_1(i, j) = \frac{R_{\text{smoothed}}(i, j)}{R(i, j)}$$

6. The order sorting boundaries are at rows  $j_b = 273, 399$

$$\text{for each } j_b \text{ set } ff_1(i, j_b) = ff_1(i, j_b) + 1.01 / 2$$

7. Threshold  $ff_1(i, j)$  to be between 0.25 and 4.0:

$$\text{if } ff_1(i, j) < 0.25 \text{ then } ff_1(i, j) = 0.25$$

$$\text{if } ff_1(i, j) > 4.0 \text{ then } ff_1(i, j) = 4.0$$

8. Produce bad pixel mask  $bp(i, j)$ :

if  $0.72 \leq ff_1(i, j) \leq 1.3$  then the pixel is “good” else it is “bad”

9. Using the “good” pixels only, pass  $C_0(i, j)$  through a 3 by 3 uniform filter to get the OBC dark count  $dc_{OBC}(i, j)$

10. Using the “good” pixels only, pass  $ff_1$  through a 3 by 3 uniform filter to get  $ff_2(i, j)$

11. Calculate  $ff_{OBC}(i, j) = \frac{ff_2(i, j)}{ff_1(i, j)}$

12. Threshold  $ff_{OBC}(i, j)$  to be between 0.25 and 4.0:

## Step 2. Process the image data.

### Inputs:

- Gain  $G(j)$  and flat field  $ff_{lab}(i, j)$ :
- The raw science data  $C(i, j, l)$
- The OBC flat field  $ff_{OBC}(i, j)$ : from Step 1
- The OBC dark count  $dc_{OBC}(i, j)$ : from Step 1
- The bad pixel mask  $bp(i, j)$ : from Step 1

### Outputs:

- The calibrated radiance  $L(i, j, l)$
- Diagnostic data (TBD)

### Process:

1. For each frame  $l$  of data, apply the radiometric calibration specified in eqs. 9. and 10.:
  - a) Subtract off the OBC dark count  $dc_{OBC}(i, j)$  from the raw counts  $C(i, j, l)$
  - b) Calculate and apply the dark pedestal shift using data from rows 2 through 14 and 467 through 479 to the counts in a.

$$p(l) = \left( \sum_{j=2}^{14} \sum_{j=467}^{479} \sum_{i=0}^{639} C(i, j, l) \right) / N, N = \text{number of points summed}$$

$$C(i, j, l) = C(i, j, l) - p(l)$$



- c) Calculate and apply the electronic panel ghost from the counts in b):

The four focal plane panels are delimited the column numbers  $i$  as follows:

$$i = 0 - 159, 160 - 319, 320 - 479, 480 - 639$$

Subtract 15% of the counts in panel 1 from each of panels 2,3,4

Subtract 15% of the counts in panel 2 from each of panels 1,3,4

Subtract 15% of the counts in panel 3 from each of panels 1,2,4

Subtract 15% of the counts in panel 4 from each of panels 1,2,3

- d) Apply the laboratory flat field  $ff_{Lab}$  to the counts in c)

$$C(i, j, l) = ff_{Lab}(i, j)C(i, j, l)$$

- e) Apply the OBC flat field  $ff_{OBC}(i, j)$  to the result in d)

$$C(i, j, l) = ff_{OBC}(i, j)C(i, j, l)$$

- f) Apply the spectral gain factor  $G(j)$  to the result in e) to get the radiance  $L$

$$L(i, j, l) = G(j) C(i, j, l)$$

- g) Interpolate the radiance  $L(i, j, l)$  from f) across the order sorting boundaries.

The order sorting boundaries are at rows  $j_b = 273, 399$

for each  $j_b$  do

$$L(i, j_b - 1, l) = \frac{2}{3}(L(i, j_b - 2, l) + \frac{1}{3}L(i, j_b + 2, l)$$

$$L(i, j_b, l) = \frac{1}{2}(L(i, j_b - 2, l) + \frac{1}{2}L(i, j_b + 2, l)$$

$$L(i, j_b + 1, l) = \frac{1}{3}(L(i, j_b - 2, l) + \frac{2}{3}L(i, j_b + 2, l)$$

- h) Trim the radiance frame down to the valid area: rows 34 to 461, columns 17 to 614

2. Calculate the diagnostic data over all the image frames (details TBD)

3. Output the data

- a) Data format: currently ENVI (TBD)

- b) Metadata: currently ENVI header (TBD)



Title: NEON ATBD: NEON Imaging Spectrometer Level 1B Calibrated Radiance		Date: 03/25/2022
NEON Doc. #: NEON.DOC.001210	Author: W. Gallery	Revision: B

**6 UNCERTAINTY**

The radiometric and spectral calibration of the airborne imaging spectrometer is traceable to standards calibrated by the National Institute of Standards and Technology (NIST). Uncertainties in the stated calibration derive from these NIST standards and are traced through the equipment and protocols used in the calibration procedures.

National Aeronautics and Space Administration’s Jet Propulsion Lab (NASA JPL) performed the initial radiometric and spectral calibration of the spectrometer prior to delivery to NEON. The uncertainties shown in **Figure 28** and **Figure 29** are the uncertainties from the JPL calibration test sets. These uncertainties are also traceable to standards defined by NIST.

**6.1 Analysis of Uncertainty**

NEON’s AOP calibration facility is currently under construction. A full uncertainty derivation has not yet been done. The analysis and derivation of the NEON radiometric and spectral calibration uncertainty will be derived as the NEON calibration test-sets are completed and accepted into operations. **Table 6** and **Table 7** give a partial list of the expected uncertainties to be included.

The NEON radiometric calibration of the imaging spectrometer is based on a NIST calibrated FEL bulb. NIST provides the spectral irradiance at a distance of 50 cm with an uncertainty that varies spectrally. Reflected radiance from a NIST traceable Spectralon reference panel is measured with a transfer radiometer. The transfer radiometer is used to transfer the NIST FEL bulb calibration to the integrating sphere used in the calibration procedure. The Spectralon panel is calibrated with respect to a NIST calibrated panel. An example of the Spectralon BRF uncertainty reported by the vendor is shown in **Figure 24**. The transfer radiometer linearity and repeatability are well-documented (Butler, et al, 1999). The transfer radiometer is used to measure the integrating sphere directly before and after the radiometric calibration of the imaging spectrometer.

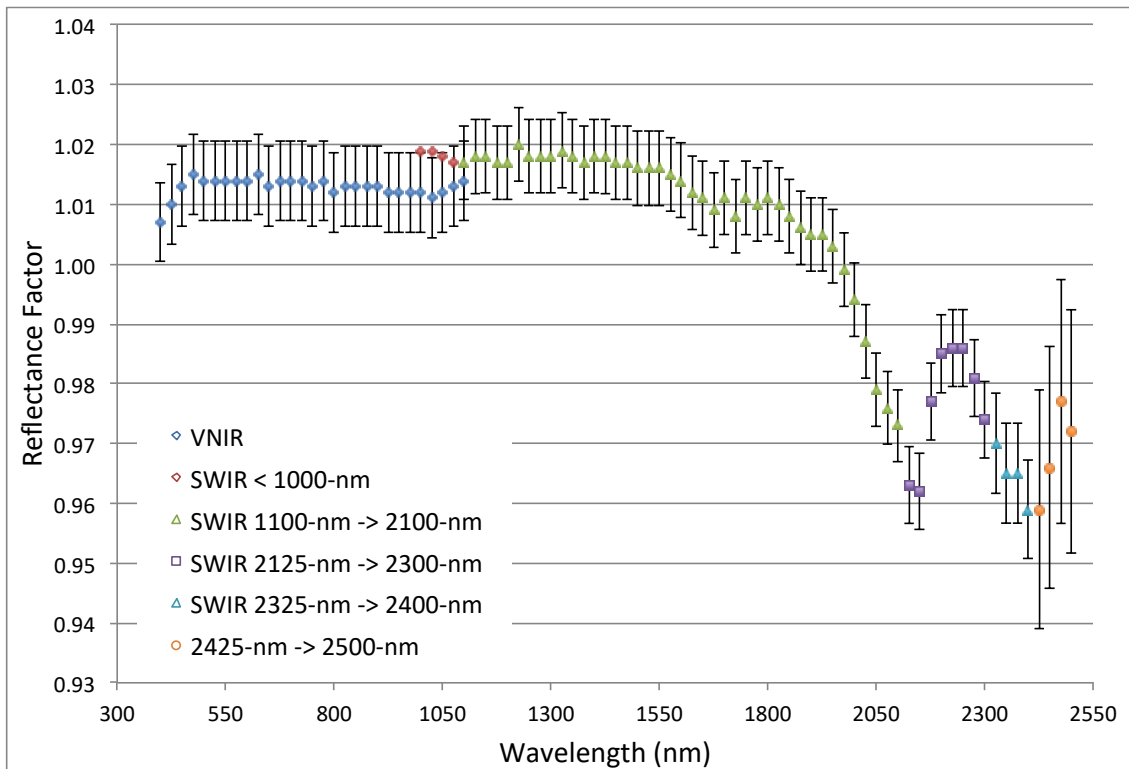


Figure 24. Spectral uncertainty in the Spectralon reference panel BRF used in the radiometric calibration of the imaging spectrometer.

Table 6. Sources of uncertainty in the radiometric calibration.

Uncertainty Source	Contribution (values are placeholders)
NIST FEL Lamp	(TBD) 1.0 %
Spectralon reference Panel	(TBD) 1.5 %
PTFE fit to multispectral BRF data	(TBD) 0.6 %
Positional accuracy of illumination geometry	(TBD) 0.5 %
Positional accuracy of viewing geometry	(TBD) 0.5 %
NTLP straylight	(TBD) 0.5 %
Stability of transfer radiometer	(TBD) 0.8 %
SIS viewing geometry	(TBD) 0.5 %
SIS stability through calibration collection	(TBD) 1.0 %
SIS uniformity over viewed area	(TBD) 0.5 %
SIS test set stray light	(TBD) 0.5 %
Spectral uncertainty (Band-center)	(TBD) 0.3 %
Spectral uncertainty (FWHM)	(TBD) 0.3 %
Combined Radiometric Uncertainty (RSS)	(TBD but expected to be better than 5 %) 2.63%

The spectral calibration of the imaging spectrometer requires the determination of the spectral response function (SRF) for each pixel. The parameters used to describe this are the band-center of the SRF, the full-width half-max (FWHM) of the SRF. The spectral band center for each pixel is determined



using emission lines while the FWHM is determined from a scanning monochromator. The monochromator is also used to determine how well the SRF can be approximated with a Gaussian curve.

Band-center uncertainty is derived from the uncertainty in the emission line spectral positions used in the spectral calibration. These lines consist of either laser lines or element (Hg, Kr, Ne, Xe, Ar) emission lines. The spectral emission lines are fit with a Gaussian curve (**Figure 25**) and used to extend the spectral calibration to the remainder of the focal plane. An example of a spectral calibration based on a Hg area-array lamp is shown in **Figure 26**.

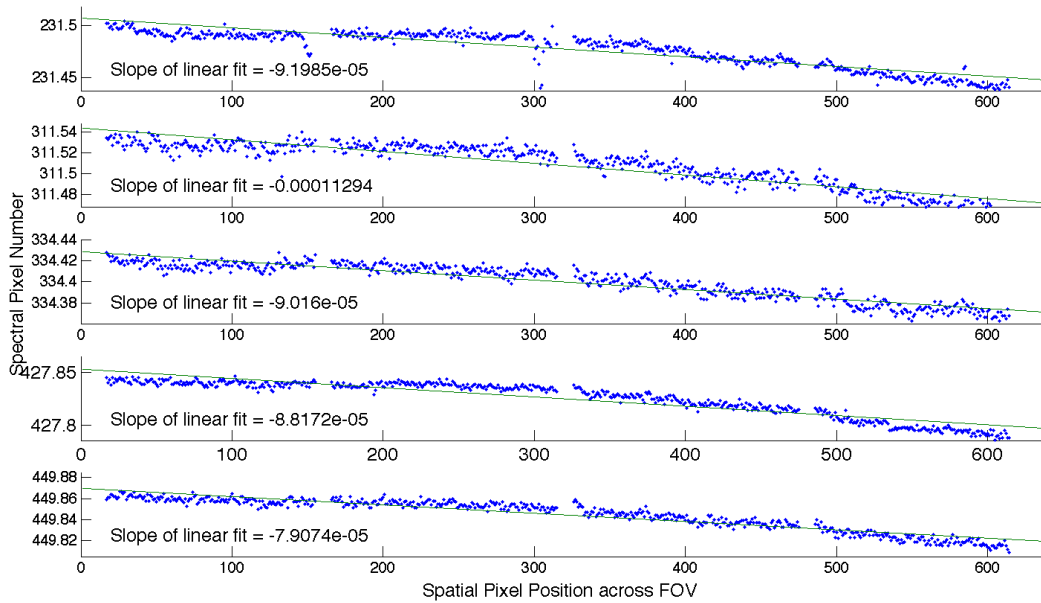


**Figure 25.** Example of spectrally fitting Gaussians to Hg area-array lamp lines through spatial pixels (x-axis) covering the FOV. The y-axis is the spectral pixel number.

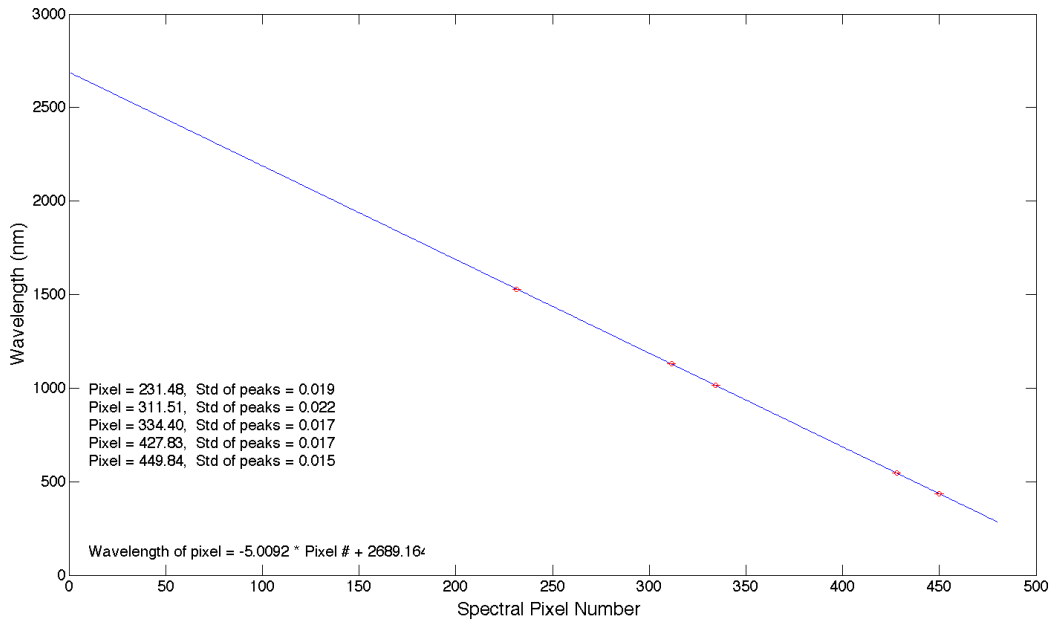


**Figure 26.** Example of extending spectral calibration to remainder of FPA based on Hg area-array lamp results.

The uncertainty of the FWHM determination is dependent on the accuracy of the scanning monochromator. This data are also used to verify the band-centers determined from the line source calibration. Use of a Hg lamp (or other elemental lamps) with multiple emission lines verify the scanning accuracy of the monochromator. An example of a derived SRF is shown in **Figure 27**.

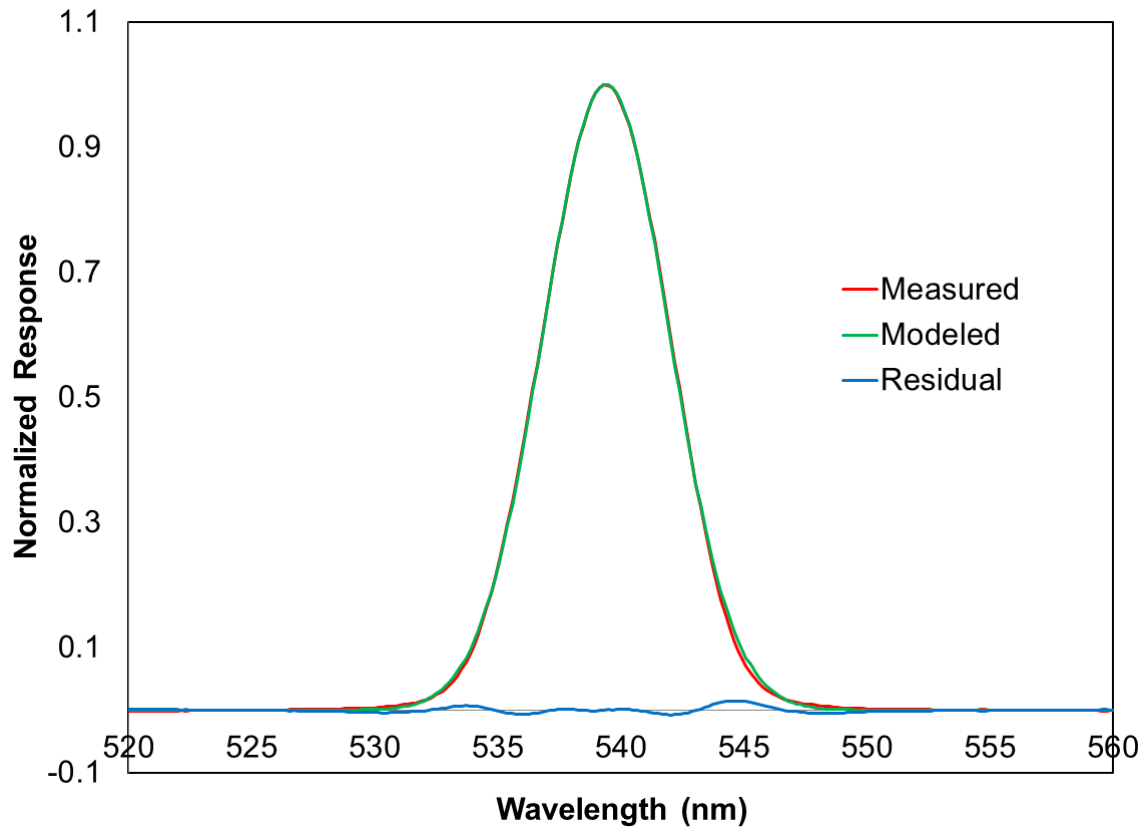


Figure 27. Normalized SRF for a single pixel compared to a modeled Gaussian SRF.

Table 7. Sources of uncertainty in the spectral calibration of the imaging spectrometer.

Uncertainty Source	Contribution (values are placeholders)
Spectral position of line source (Laser or element)	(TBD)
Centroiding FPA pixels illuminated	(TBD)
Extrapolation to remaining FPA pixels	(TBD)
Spectral accuracy of monochromator	(TBD)
<b>Combined Spectral Uncertainty (RSS)</b>	<b>(TBD)</b>



## 6.2 Reported Uncertainty

This section gives the results of JPL's analysis of the radiometric and spectral calibration provided at the time of delivery of the instrument delivery. The uncertainty in the radiometric calibration for each channel is shown in **Figure 28**. The spectral calibration uncertainty is reported in units of nanometers for every channel of the spectrometer and is shown in **Figure 29**.

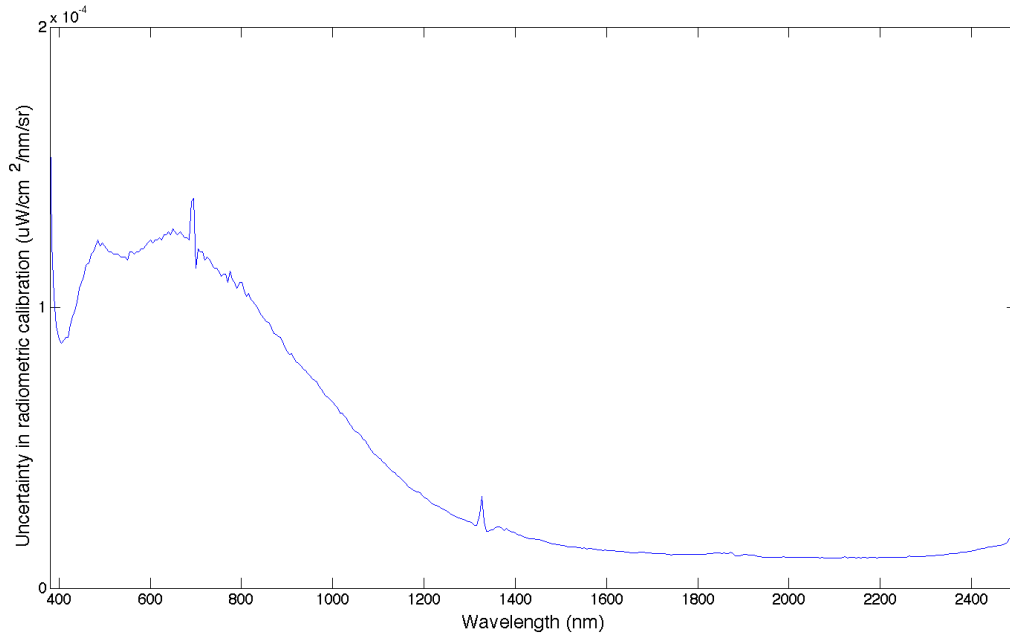
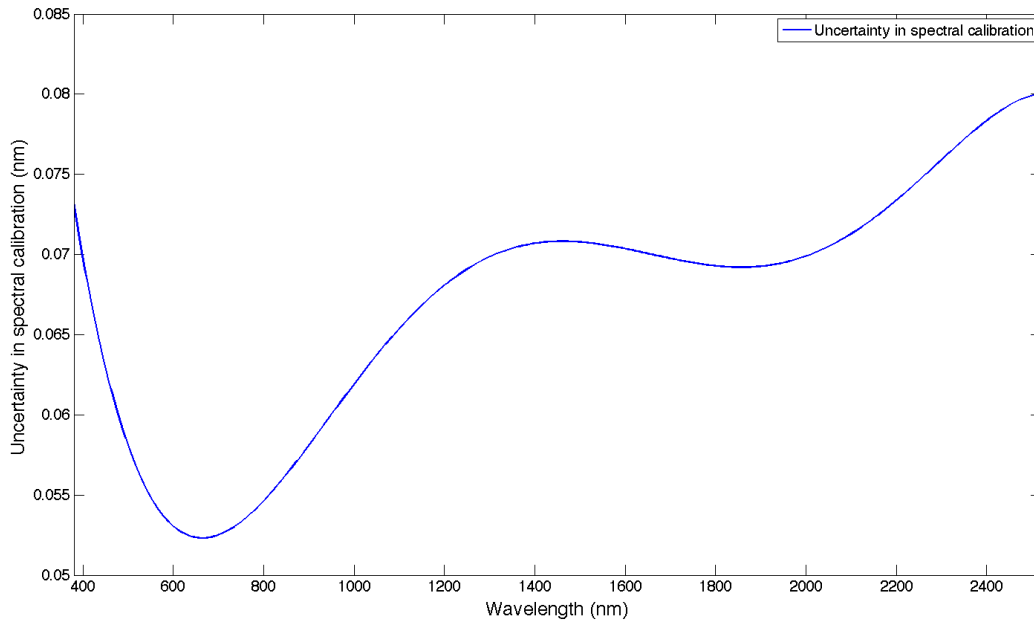


Figure 28. Radiometric calibration uncertainty based on the NIST traceable calibration protocol.



**Figure 29.** Spectral calibration uncertainties for pixel band-centers derived from spectrally calibrating the imaging spectrometer with Laser lines injected into an integrating sphere.

The uncertainties stated here are tied to the JPL’s calibration method. They also will be carried through into the accuracy of the subsequent data products derived from the calibrated radiance reported by the imaging spectrometer.



Title: NEON ATBD: NEON Imaging Spectrometer Level 1B Calibrated Radiance		Date: 03/25/2022
NEON Doc. #: NEON.DOC.001210	Author: W. Gallery	Revision: B

**7 VALIDATION AND VERIFICATION**

The radiance calibration algorithm describes the procedure for converting raw DN to calibrated, at-sensor spectral radiance. It is validated through several independent methods. The initial process is to apply the algorithm to the dataset used to generate the calibration files (the flat field and the radiometric calibration coefficients). The resulting radiance is compared to the known value of the source used to determine the calibration files.

If the algorithm correctly reproduces the source radiance, the algorithm is applied to other datasets of the same known laboratory source from different times. This extension tests the stability of the instrument, the algorithm, the laboratory sources, and the alternative instruments used to determine the radiance output of the source.

The algorithm is then applied to datasets collected in the field. Typically, natural targets in the field have an unknown radiance; this is why airborne spectrometer measurements are required. This is mitigated through several mechanisms. During most flight campaigns, reflectance targets of a known or measured reflectance are imaged by the airborne spectrometer. The radiance at the imaging spectrometer is modeled using a radiative transfer code with the atmospheric characterization determined from sun photometer measurements and the known reflectance of the target. This provides an independent verification of the laboratory calibration in field conditions.

The NIS radiance calibration algorithm is also verified through dedicated vicarious calibration test flights. These flights typically occur shortly after integration into the airplane. Natural targets historically used for satellite calibration, such as desert playas, are used due to their highly desirable – and well known - characteristics. Dry lakebeds are chosen which exhibit a high degree of spatial uniformity in addition to a strong flat spectral reflectance. This provides a high quality target for an independent method of radiometrically calibrating or verifying the sensor calibration

The combination of these methods provides a robust method of verify sensor performance as well as the algorithm used to convert the raw data to radiance. Long-term behavior of the sensor during a flight season will be monitored using the on-board calibration system. If this indicates the sensor or the calibration is no longer valid, a decision will be made to collect a vicarious calibration dataset in the field or return the instrument to the lab for further calibration or repair.



**neon**  
Operated by Battelle

<i>Title:</i> NEON ATBD: NEON Imaging Spectrometer Level 1B Calibrated Radiance		<i>Date:</i> 03/25/2022
<i>NEON Doc. #:</i> NEON.DOC.001210	<i>Author:</i> W. Gallery	<i>Revision:</i> B

## 8 SCIENTIFIC AND EDUCATIONAL APPLICATIONS

Currently the calibrated but non-orthorectified radiance data described here is considered an intermediate product and not an official NEON distributed product.



Title: NEON ATBD: NEON Imaging Spectrometer Level 1B Calibrated Radiance		Date: 03/25/2022
NEON Doc. #: NEON.DOC.001210	Author: W. Gallery	Revision: B

**9 FUTURE MODIFICATIONS AND PLANS**

The algorithm detailed here for processing raw digital counts to calibrated radiance is derived from the initial JPL algorithm. The algorithm will be updated as NEON learns about new characteristics of the focal plane and the imaging spectrometer instrument resulting in modifications to the equations applied as well as to the format of the input files and output from this algorithm. A list of potential changes is given below:

- Currently, only the second dark offset is used to correct the detector bias. This will be modified to include the first dark offset. Potential changes between these dark collects will be handled by linearly interpolating between the two and applying the result to the science frame of interest.
- Bad pixels will also be determined using dark collect and science frames (currently only the OBC mid data is used).
- The bad pixel mask will be used to mark pixels for interpolation. These pixels will be flagged in the output of this algorithm.
- Work is being done to quantify the effects of the Electronic Panel Ghost and Dark Pedestal Shift for improved characterization and correction.
- An analysis will be made into the most suitable output format, e.g., ENVI (current), HDF5, or an alternative.
- The data across focal plane boundaries (the order sorting filter boundaries and the read-out boundaries (taps)) shows significant discontinuities. We will determine the best way to handle the data at these boundaries. These pixels may have to be interpolated for some light levels while the laboratory calibration may be able to handle some situations.
- Some flight line diagnostic data is currently calculated but not stored. We will determine the best procedure for handling of this potentially valuable data.



## 10 BIBLIOGRAPHY

Green, R. et al. (1998), *Imaging spectroscopy and the airborne visible/infrared imaging spectrometer (AVIRIS)*, Remote Sensing of Environment, 4257(98). [online] Available from: <http://www.sciencedirect.com/science/article/pii/S0034425798000649> (Accessed 20 February 2013)

Hamlin, L., R. O. Green, P. Mouroulis, M. Eastwood, I. McCubbin, D. Wilson, D. Randall, M. Dudik, C. Paine, June 2010, *Imaging Spectrometer Science Measurements for Terrestrial Ecology: AVIRIS and the Next Generation AVIRIS: Characteristics and Development Status*, [http://esto.nasa.gov/conferences/estf2010/presentations/Hamlin\\_Green\\_ESTF2010\\_B4P4.pdf](http://esto.nasa.gov/conferences/estf2010/presentations/Hamlin_Green_ESTF2010_B4P4.pdf)

Butler, James J., B. Carol Johnson, Steven W. Brown, Howard W. Yoon, Robert A. Barnes, Brian L. Markham, Stuart F. Biggar, Edward F. Zalewski, Paul R. Spyak, John W. Cooper, Fumihiko Sakuma, *Radiometric measurement comparisons using transfer radiometers in support of the calibration of NASA's Earth Observing System (EOS) sensors*. Proc. SPIE 3870, Sensors, Systems, and Next-Generation Satellites III, 180 (December 28, 1999); doi:10.1117/12.373186

NEON AOP video: [http://www.youtube.com/watch?feature=player\\_detailpage&v=SehdS6y\\_mjM](http://www.youtube.com/watch?feature=player_detailpage&v=SehdS6y_mjM)

## 11 APPENDIX A AOP ABBREVIATIONS AND GLOSSARY

This appendix defines abbreviations and terms related to the AOP instruments and operations, particularly as related to GNSS geolocation and to airborne lidar.

### Abbreviations

**Table 8.** Abbreviations.

Term	Definition
<a href="#">ALTM</a>	Airborne Laser Terrain Mapper: Optech’s Gemini Lidar system
<a href="#">ALTMW</a>	Airborne Laser Terrain Mapper Waveform Digitizer: <a href="#">Optech</a> ’s waveform digitizer
<a href="#">AOP</a>	Airborne Optical Platform: NEON’s airborne sensor suit consisting of: the georeferencing system (POSAV) the waveform lidar (ALTM) the waveform digitizer (ALTMW) the imaging spectrometer (NIS) the digital camera D-8900
<a href="#">CORS</a>	Continuously Operating Reference Stations: a set of fixed ground stations whose locations are precisely known
<a href="#">ENVI</a>	A commercial software package, the Environment for Visualizing Imagery, used for image analysis, particularly suited for satellite imagery
<a href="#">D-8900</a>	<a href="#">Optech</a> ’s airborne digital camera used on the AOP
DEM	Digital Elevation Model, see Section Digital Elevation DEM
<a href="#">DGPS</a>	Differential Global Positioning System
DP	Data Product
DVU	Design Verification Unit: the first NIS unit
<a href="#">GALILEO</a>	The EU GNSS
<a href="#">GEMINI</a>	<a href="#">Optech</a> ’s discrete imaging lidar system used on the AOP
<a href="#">GLONASS</a>	The Russian GNSS
GLT	Geometric Lookup Table
GNSS	Global Navigation Satellite System: generic term
<a href="#">GPS</a>	Global Positioning Satellite: the US GNSS
IGM	Input Geometry Matrix
IMU	Inertial Measurement Unit: Applanix’s inertial navigation hardware, part of POSAV
LMS	Lidar Mapping Suite: <a href="#">Optech</a> ’s software to geolocation the lidar pixels
LTM	Laser Terrain Mapper: generic term



Title: NEON ATBD: NEON Imaging Spectrometer Level 1B Calibrated Radiance		Date: 03/25/2022
NEON Doc. #: NEON.DOC.001210	Author: W. Gallery	Revision: B

Term	Definition
<a href="#">NAD83</a>	<b>National American Datum of 1983</b>
NIS	<b>NEON Imaging Spectrometer:</b> <b>NISDVU</b> refers to the first NIS sensor, the <b>Development Unit</b> <b>NIS1</b> refers to the second NIS sensor, after DVU. <b>NIS0</b> also refers to the DVU
OBC	<b>On Board Calibrator:</b> a calibration source (lamp) which is part of the NIS and provides two levels of illumination, mid- and high-level.
OBS	<b>Observation geometry parameter</b>
ORT	<b>OrthoRectified imagery Table</b>
PDOP	<b>Positional Dilution Of Precision</b>
POS	<b>Position and Orientation System</b>
<a href="#">POSAV</a>	<b>Position and Orientation System AViation:</b> Applanix's GNSS and inertial hardware to record the trajectory of an airplane
POSGNSS	<b>Position and Orientation System Global Navigation Satellite System:</b> Applanix's software to process GNSS data from POSAV
POSPAC MMS	<b>Position and Orientation System Post Processing Package Mobile Mapping Suite:</b> Software for processing POSAV data
POSPROC	<b>Position and Orientation System Post Processing:</b> the Software to process the IMU data
RINEX	<b>Receiver Independent Exchange Format:</b> a standard file format for GNSS
sbet	<b>smoothed best estimate of trajectory:</b> the aircraft trajectory file output by PSOPAC MMS
UQ	<b>Unquantifiable Uncertainty</b>



Title: NEON ATBD: NEON Imaging Spectrometer Level 1B Calibrated Radiance		Date: 03/25/2022
NEON Doc. #: NEON.DOC.001210	Author: W. Gallery	Revision: B

**Glossary**

**Table 9.** Glossary.

Term	Definition
<b>Radiance Calibration</b>	
flat fielding	Correcting the output of an image detector for variations in the detector sensitivity.
bad pixel mask	A focal plane mask indicating which pixels are dead (no signal) or bad (intermittent or out-of-range signal)
order sorting filter	
<b>Geolocation</b> (see Section Geolocation for a more detailed discussion)	
geoid	A spherical harmonic model of the Earth's gravitational potential
geolocation	The process of referencing a data point or an image in terms of a map projection or coordinate system. Also known as orthorectification.
georeferencing	See geolocating, which is the preferred term.
orthorectification	The process of geolocating a point or area and matching it to another point or area, e.g. to a point on another image or map.
<b>Flight operations</b>	
campaign	The AOP operations for a single season, e.g., 2012.
deployment	Continuous flight operations over a single site for a limited time, e.g., flight operations over Harvard Forest from May 4 to May 10, 2012. A campaign consists of a number of deployments.
Flight	A single flight from/to the FBO and including a number of flight lines
flight line	A segment of a flight along a straight line during which Lidar and NIS observations are taken. Science data is only taken along a flight line.
FBO	<b>Fixed Base Operator:</b> the aircraft support at a fixed location, e.g., Grand Junction, CO. Support includes hanger space, fuel, power ...

**Recommended Usage**

There are certain terms in the geolocation community that are closely related but often confused. This section attempts to clarify these terms and set out the recommended usage at NEON.



Title: NEON ATBD: NEON Imaging Spectrometer Level 1B Calibrated Radiance		Date: 03/25/2022
NEON Doc. #: NEON.DOC.001210	Author: W. Gallery	Revision: B

## Geolocation/Orthorectification/Georectification

Note: parts of this section are taken from [Imagery Speaks](#). See also [ERDAS Field Guide, December 2010](#)

- **Geolocate:**
- **Georectify:** To take an image that has not been adjusted to be in a known coordinate system, and put it into a known coordinate system. Usually this means taking an image that is in its original geometry, and mapping it into a specific projection. There are different ways to do this. Perhaps the most common way is to identify a set of points in the image for which the latitude and longitude or map coordinates are known, and use them to warp the image into a map projection.
- **Georeference:** To take an image that is already in a known coordinate system, and provide the information necessary for software to understand which coordinate system it is in.
- **Geocode:** Same as georeference.
- **Geometrically Correct:** Same as georectify.
- **Orthorectify:** To take an image in its original geometry and very accurately adjust it so that it is in a known coordinate system, with distortions due to topographic variation corrected. An orthorectified image has uniform scale throughout the image. A DEM (and by this, I mean an image in which the pixel values represent the ground elevation above sea level) is required for true orthorectification.

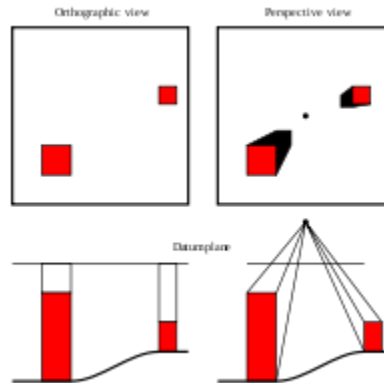


**Figure 30.** Orthorectification - each point (pixel) in the image is from a perpendicular (orthogonal) perspective. As you look down at each pixel it's as if you are looking straight down on that pixel. Left image is orthorectified; right is not.

### Recommended usage:

- Orthorectify



## Digital Elevation

The following three terms are closely related and sometimes (mistakenly) used interchangeably

- **DEM:** digital elevation map. Regularly gridded 2.5D representation of a three-dimensional scene whose per-pixel values are referenced to Mean Sea Level. DTM and DSM are specific DEM types.
- **DTM:** digital terrain map. Bare earth DEM, where things like trees and buildings have been removed.
- **DSM:** digital surface map. Equivalent to shrink-wrapping a 3D scene, so you see the tops of trees, buildings, etc.

### Recommended usage:

- Use DEM as a generic term for either a DTM or a DSM.
- Use DTM or DSM when referring specifically to either a terrain or surface map.